FLUORESCENCE AND ELASTIC SCATTERING FROM LASER DYE-FILLED CAPILLARIES

by

Edward Michael Sekerak

A Thesis Submitted to the Faculty of the

DEPARTMENT OF OPTICAL SCIENCES

In Partial Fulfillment of the Requirements
For the Degree of

MASTER OF SCIENCE

In the Graduate College

THE UNIVERSITY OF ARIZONA

1989

REPORT DOCUMENTATION PAGE

Form Approved OMB No. 0704-0188

1a. REPORT SECURITY CLASSIFICATION UNCLAS	1b. RESTRICTIVE MARKINGS NONE
2a. SECURITY CLASSIFICATION AUTHORITY N/A	3. DISTRIBUTION/AVAILABILITY OF REPORT N/A
2b. DECLASSIFICATION/DOWNGRADING SCHEDULE N/A	
4. PERFORMING ORGANIZATION REPORT NUMBER(S) N/A	5. MONITORING ORGANIZATION REPORT NUMBER(S) N/A
6a. NAME OF PERFORMING ORGANIZATION U.S. ARMY UNIVERSITY OF ARIZONA 6b. OFFICE SYMBOL (If applicable) N/A	7a. NAME OF MONITORING ORGANIZATION N/A
6c. ADDRESS (City, State, and ZIP Code) Optical Sciences Center University of Arizona Tucson, AZ 85721	7b. ADDRESS (City, State, and ZIP Code) N/A
8a. NAME OF FUNDING/SPONSORING ORGANIZATION U.S. Army, TAPC 8b. OFFICE SYMBOL (If applicable) N/A	9. PROCUREMENT INSTRUMENT IDENTIFICATION NUMBER N/A
8c. ADDRESS (City, State, and ZIP Code) ATTN: TAPC-OPB-D 200 Stovall Street Alexandria, VA 22332-0444	10. SOURCE OF FUNDING NUMBERS PROGRAM ELEMENT NO. N/A PROJECT NO. N/A TASK NO. N/A WORK UNIT ACCESSION NO N/A
11. TITLE (Include Security Classification) FLUORESCENCE AND ELASTIC SCATTERING FROM LASER DYE-FILLED CAPILLARIES	
12. PERSONAL AUTHOR(S) SEKERAK, Edward M. (CPT)	
13a. TYPE OF REPORT MS Thesis	13b. TIME COVERED FROM 880915 TO 890823
14. DATE OF REPORT (Year, Month, Day) 890823	15. PAGE COUNT 71
16. SUPPLEMENTARY NOTATION Master of Science (MS) Thesis for U.S. Army Advanced Civil Scholling Program	

17. COSATI CODES		
FIELD	GROUP	SUB-GROUP

18. SUBJECT TERMS (Continue on reverse if necessary and identify by block number)
Spectroscopy, Capillary Zone Electrophoresis, Laser Dye, Coumarin 7, He Cd Laser

19. ABSTRACT (Continue on reverse if necessary and identify by block number)

(See ABSTRACT IN THESIS)

20. DISTRIBUTION/AVAILABILITY OF ABSTRACT ☒ UNCLASSIFIED/UNLIMITED ☐ SAME AS RPT ☐ DTIC USERS	21. ABSTRACT SECURITY CLASSIFICATION UNCLAS
22a. NAME OF RESPONSIBLE INDIVIDUAL CPT EDWARD M. SEKERAK	22b. TELEPHONE (Include Area Code) AV 254-3573/4387 22c. OFFICE SYMBOL CSSD=KTU

DD Form 1473, JUN 86 *Previous editions are obsolete.* SECURITY CLASSIFICATION OF THIS PAGE

STATEMENT BY AUTHOR

This thesis has been submitted in partial fulfillment of requirements for an advanced degree at The University of Arizona and is deposited in the University Library to be made available to borrowers under rules of the Library.

Brief quotations from this thesis are allowable without special permission, provided that accurate acknowledgment of source is made. Requests for permission for extended quotation from or reproduction of this manuscript in whole or in part may be granted by the head of the major department or the Dean of the Graduate College when in his or her judgment the proposed use of the material is in the interests of scholarship. In all other instances, however, permission must be obtained from the author.

SIGNED: Edward M. Sekera

APPROVAL BY THESIS DIRECTOR

This thesis has been approved on the date shown below:

William S. Bickel
Professor of Physics
Director

Aug 23/89
Date

Roland V. Shack
Professor of Optical Sciences
Co-Director

8/23/89
Date

ACKNOWLEDGMENTS

I express my most sincere thanks to Dr. William S. Bickel for his insightful guidance, never-ending encouragement, and contagious enthusiasm. His relationship to me as mentor, friend, and professor made this thesis both exciting and rewarding. Though the thesis work is over, I will always keep the memories of the comradery we shared during some of those long days and late nights.

I gratefully thank Adele "the wife" for her love, and also Adele "the graphic designer" for her help with illustrations. To have had both her emotional support and artistic abilities contribute to the completion of this thesis was extremely meaningful to me. Many thanks to Cassandra, Angela, and Nina (my little Airborne Rangers) for the joy they brought me during the tough times and for helping me keep things in perspective.

I thank Dr. Roland Shack for his fascinating courses and philosophies about learning. I also thank John Pattison for his electronic expertise; Tom Wentzel and Dave Abromson for their assistance with the computer; Ka Chun Yu and Jim Gilmore for their contributions in the course of their independent studies; Mary Turner for her advice as a "big sister"; and all of the above for their friendship.

Additionally, I thank Elaine Segura for her editorial expertise and Rosie Miller for helping me put this thesis in its final form.

TABLE OF CONTENTS

LIST OF ILLUSTRATIONS

ABSTRACT

We investigated the elastic scattering and fluorescence from laser dye solutions inside 5000, 1100, and 96.5 micron inner-diameter hollow-core capillaries. Incident 4416 Å laser illumination of Coumarin 7 dye dissolved in ethanol caused fluorescence from approximately 4600 to 6000 Å. This was studied over an angular range from 0^{o} to 360^{o}. A light scattering nephelometer coupled with a spectrometer gave intensity measurements as functions of wavelength (at fixed detection angles) and angle (at fixed wavelengths), while the illumination source, dye-filled capillary, and detector remained stationary. We saw capillary size and detection-angle dependence of the fluorescence and elastic scattering. Results show that angular variations of the elastic scattering and emitted fluorescence can be used to determine an optimum detection angle from the capillary with respect to the incident illumination direction. This work is important in the design and execution of Capillary Zone Electrophoresis (CZE) experiments.

CHAPTER 1

INTRODUCTION

Capillary Zone Electrophoresis (CZE) is a newly developing field of analysis whereby laser excitation causes biological materials in a hollow core capillary to fluoresce. The fluorescence is then studied to identify constitute elements and/or characterize specific properties in the core materials under investigation. CZE experiments conducted up to the present time, such as those by Green[1] and Wallingford,[2] have not taken optical considerations of the capillary and core material fully into account. Yet these considerations are important in determining an optimum detection angle from the core material, with respect to the direction of the incident illumination. The purpose of this research was to design and build an experimental workstation to study the fluorescence from excited core materials in capillaries and identify some effects which should be considered in CZE experiments.

Measurement of light from a sample-filled capillary involves the detection of scattered light. Scattered light occurs when electromagnetic energy (photons) incident upon matter causes the electric charges, which comprise matter, to oscillate and radiate in all directions. Incident photons can scatter elastically with negligible energy loss or inelastically, where some of their energy is absorbed. When absorption occurs, incident photons are absorbed. This causes the atoms or molecules in the material to become excited and photons with longer wavelengths are reradiated as the material relaxes back to its ground state. Inelastic scattering" refers to this process. The fluorescence emitted from the excited core material in

capillaries is produced by this inelastic scattering process.

Light detected from a sample-filled capillary therefore originates from two sources: from the incident illumination, which is elastically scattered by the capillary and from the fluorescence, which is emitted (inelastically scattered) from the core material. The elastic scattering can be used to determine the capillary's geometry, surface imperfections, and refractive index.[3,4] However, the fluorescence contains the information about the core material under study.

The elastic scattering from cylindrical capillaries is roughly confined to a plane. If the incident illumination is directed horizontally across a vertical capillary, the elastic scattering plane will be normal to the capillary. Intensity measurements show that the elastic scattering is not uniform and has angular oscillations which can vary by several orders of magnitude. These angular oscillations depend upon the relative sizes of the capillary and the illuminating wavelength. Capillaries with diameters much larger than the incident wavelength exhibit high frequency angular oscillations. As the size of the capillary diameter decreases, the angular oscillation frequency decreases and the amplitude increases.[3]

The fluorescence is not limited to a plane, as is the elastic scattering, and propagates in all directions. During excitation, the sample material absorbs some incident radiation. The excited material decays to its initial ground-state condition and emits photons with longer wavelengths than the absorbed photons. The fluorescence mechanism, being different than elastic scattering, is expected to radiate uniformly in all directions. However capillary geometry, the volume of the region where excitation occurs, and the absorptive/fluorescent characteristics of the material under study prevent uniform fluorescence from occurring.

Much experimental and theoretical research has been done to study fluorescent materials in spherical systems. Benner[5] demonstrated that small dye-filled

polystyrene spheres acted as resonating cavities to produce enhancement of fluorescence in certain directions at wavelengths that satisfy resonating mode conditions. Additional work, which showed resonant enhancement of fluorescent spherical systems, was done by Arnold,[6] Lin,[7] and Biswas.[8] Kratohvil[9] showed angular intensity variations in the polarized fluorescence from dyes in 0.3 micron diameter latex spheres. Theoretical models for fluorescent materials in spherical systems were developed by Chew.[10,11] Numerical computations by Chew[12] and Kerker[13] mathematically explained the uniform intensity from incoherent fluorescence and the variable intensity from coherent fluorescence observed experimentally.

Although some of the results from the investigation of spherical systems has direct applications to CZE, information regarding the fluorescence in actual cylindrical systems is not nearly as abundant. Chew[14] developed a model that outlined the transition from structured fluorescence oscillations to isotropic fluorescence as the size of the capillary's inner diameter became large with respect to the incident excitation wavelength. Owen[15] investigated the fluorescence from a solid glass fiber that was coated with a fluorescent dye. The first significant study of fluorescence in hollow core capillaries has been done by Abromson.[16] Abromson separately used a spectrometer to study the wavelength dependence at fixed detection angles and a nephelometer with bandpass filters to study angular intensity variations within discrete wavelength regions.

Currently, researchers conducting CZE experiments use sample-filled capillaries with inner diameters ranging from 100 microns down to 12.7 microns. They hope to extend these experiments to capillary inner diameters as small as one micron.[17] Measurements are routinely made at 90° detection angles. No apparent study of the sample-filled capillary's optical characterisitics has been made to determine if this

detection angle is best. Since the fluorescence intensity is essentially proportional to the small amount of excited core material, the intensity decreases and the detection of fluorescence becomes increasingly difficult as smaller capillary sizes are used. This research shows that the elastic scattering and fluorescence emission from capillary systems is complex and should be studied in order to optimize the design and execution of CZE-type experiments.

CHAPTER 2
DESCRIPTION OF THE EQUIPMENT

The system required to perform these experiments was assembled from equipment available in the University of Arizona Physics Department. The individual components required varying levels of repair, alignment, and modification, since some of the equipment had not been used for more than six years; others had not been used in the manner intended for this experiment; and all the individual pieces of equipment had to operate collectively in the resultant system.

2.1. Overview

The experimental system is illustrated in Figure 1. A light scattering nephelometer and a spectrometer were used in combination to detect light from a laser-dye-filled capillary as a function of illumination (detection) angle and wavelength. (A nephelometer, or cloud meter, was initially used to study light scattering from "clouds" of water droplets.) The system was designed to provide maximum flexibility for this research and future work. It can accomodate different light sources, samples, optics, and measuring techniques.

An Omnichrome He-Cd 50 mW laser (Model 456XM) provided a 4416 Å beam for incident illumination. The laser beam passed through a spatial filter and collimator (two reversed 10X microscope objectives with a 25 μm pinhole in between) to improve the beam quality and provide a nearly uniform cross-sectional beam with a 4 mm spot size at the entrance aperture of the nephelometer. The laser beam was stable well within the noise limitations of the system after a 10-minute warmup period.

The laser and spatial filter/collimator were semi-permanently mounted on an aluminum bracket. A mirror, mounted on a unidirectional translation stage after the spatial filter/collimator, could be moved in or out of the laser beam in order to send the beam to other experiments. Mirror movement was limited by a teflon screw stop attached to the translation stage. This stop ensured that the laser beam was directed precisely to the nephelometer after any mirror movement.

The nephelometer was an optical axicon arrangement originally developed and constructed by Bickel.[18] The axicon could measure a 0° - 360° angular range of scattered light (except for a blocked region from 177° to 183°) without moving the incident light source or detector. A lens on an external mount placed before the axicon focused the beam onto the sample. The 4-mm-diameter entrance aperture transmitted the center portion of the beam to ensure nearly uniform illumination across the sample when the external focusing lens was not used. The input mirrors aligned the incident illumination with the axicon's stationary and rotating mirrors.

The dye-filled capillary is placed at the axicon's center of rotation and illuminated by the incident beam, which is directed horizontally across the capillary at an angle determined by the the axicon's mirrors. The capillary then scatters and/or emits light in all directions. Changing the angle of illumination with respect to the capillary-detector direction effectively changes of the angle of detection. The detector and its associated input optics remain stationary while detecting light in any angular direction.

The input optics to the spectrometer consisted of a slit aperture and two achromatic lenses. The slit aperture defined the angular resolution of light transmitted from the capillary to the detector. Light from the capillary was collected and collimated by the first lens. The second lens focused the light onto the entrance slit of the spectrometer.

A Robin mount spectrometer was used to spectrally analyze the light from the capillary. Light from the entrance slit was imaged by a concave reflective diffraction grating through the spectrometer's exit slit and detected by a photomultiplier tube.

Signals from the photomultiplier tube could be measured two ways. One method was pulse counting. It was used during the initial familiarization and calibration of the spectrometer. Equipment needed for pulse counting included a linear amplifier and single channel analyzer (Tennelec Model TC 214), to amplify the signal pulses and discriminate them from noise pulses; a counter/timer (Tennelec Model TC 555A), to acquire the number of pulses per specified unit of time or time per specified number of pulses; and a digital signal analyzer (Tracor Northern Model NS-575A), to store the number of pulses counted for several different scans, perform processing operations to compare and analyze data, and transmit the data to a strip chart recorder for a hard copy record of the experiment.

The other method was current detection with a picoammeter. The negative photomultiplier current was converted by a picoammeter to an output voltage. The voltage was then sent to a strip chart recorder and a computer via an analog to digital (A/D) data acquisition board, either simultaneously or independently. The chart recorder provided an instantaneous record of the experiment, while the computer furnished automatic data storage, analysis, and retrieval. Current detection was used for most of the measurements in these experiments.

2.2. Axicon

Light measurement as a function of angle requires movement of either the illuminating source or the detector and its associated optics over the angular region of interest. Bickel's axicon optical system for light scattering experiments rotated

the incident laser beam across the sample-filled capillaries without physically moving either the laser or the spectrometer.

Figure 2 depicts the optical axicon system used in the experimental setup. The incident laser beam entered the 4-mm-diameter aperture A1. A focusing lens could be mounted in front of A1 if a smaller beam spot size on the capillary was needed. Otherwise, the central portion of the incident beam was transmitted through A1 to provide a beam that was fairly uniform in intensity over the much smaller capillary cross-sectional area. The input mirrors M1 and M2 directed the beam through alignment aperture A2 to mirror M3, which was rigidly attached to an arm connected to the axicon's base.

Mirror M3 reflected the beam down the axis of rotation to mirror M4 and diagonally downward to mirror M5. Both M4 and M5 were mounted on an arm joined to the rotating platform. (This arm blocks the transmission of light from the capillary to the spectrometer between approximately 177° and 183°.) Mirror M5 sent the beam horizontally across the rotating table and through the capillary. A beam stop placed at point P prevented the undeflected beam from entering the spectrometer's input optics directly and minimized reflection of the laser beam back through the capillary. When properly aligned, the beam ray path M3-M4-M5-capillary-P lies in a single plane for any angular movement of the rotating platform.

The polarization orientation of the illumination at the capillary depends on the angular movement if the incident light is either linearly or elliptically polarized. Circularly polarized and unpolarized light are independent of angular movement and therefore remain in their original states at the capillary. (The laser used in this experiment produced an unpolarized beam. The resultant beam transmitted through the axicon was examined with a linear polarizer and found to be essentially

unpolarized throughout the axicon's entire angular movement.)

The axicon required repair, realignment, and modification prior to use in the experiment. We mounted M1 and M2 on an additional base to orient the laser beam correctly; reattached M3, M4, and M5 firmly to their original adjustable mounts; and installed the two apertures (A1 and A2) and the beam stop, which were newly designed for application to this particular setup.

The laser beam maintains a constant relative position on the capillary during movement of the rotating platform only if the axicon is properly aligned. Axicon alignment was accomplished by removing M4 and placing a flat mirror on the rotating platform. The beam, which was initially reflected by M3 down the axis of rotation to the rotating platform, was reflected by the flat mirror back through the axicon mirrors and apertures to the laser. As the table is rotated through all angles, the beam will remain reflected back on itself only if the beam lies exactly on the axis of rotation. After adjusting M1, M2, and M3 to send the beam down the axis of rotation, M4 was replaced. M4 and M5 were then adjusted to attain the required beam height and make sure the beam intersected the axis of rotation horizontally across the diameter of the rotating platform.

The circular rotating platform was mounted on a roller-bearing assembly and turned by a gear shaft. A 22:1 gear reduction transfer mechanism connected to a 200 step/revolution stepper motor was constructed to turn the rotating platform. This arrangement gave an angular resolution of 0.014 degrees/step, or 73.3 steps/degree. A stepper motor driver controlled the stepper motor. It had controls for bi-directional movement of the rotating platform; variable motor speed control; precise number of steps per movement; and continuous, momentary, and single step control of the motor.

The rotating platform's angular position was monitored by a 10-turn

potentiometer coupled to the platform's gear shaft with an "O-ring" belt. A 15 volt power supply provided the input signal to the potentiometer and the output was recorded by one of the computer's A/D channels. The desired output voltage range was set by adjusting the potentiometer at the starting angle. Voltage output would increase or decrease corresponding to the rotation direction of the platform. A 360° scan could be made in any direction or a ±180° bi-directional scan from any initial angle within the turn limitation of the potentiometer.

2.3. Input Optics

The cylindrically-shaped capillaries approximated line sources and by themselves could not fully illuminate the spectrometer's grating. The spectrometer's input optics were designed specifically to optimize the light gathered from the capillaries and transfer it to the spectrometer. Image quality, although important, was not as significant a concern as maximizing the light entering the spectrometer. (In fact, spectral line shapes observed with and without the input optics were the same.)

The input optics consisted of a slit aperture and two achromatic lenses. The slit aperture defined an acceptance angle of approximately one degree from the dye-filled capillary to the input optics. Selection and placement of the two achromatic lenses was determined by the fluorescent light (first-order ray approximation), as opposed to the much stronger elastic scattering (Gaussian beam propagation). The resultant exit angle of the input optics (f/12.7) was slightly smaller than the acceptance angle of the spectrometer (f/12.5) in the horizontal plane about the optical axis. This ensured the light transmitted from the axicon nearly filled the grating, without losing light by overfilling the grating. Ray trace diagrams are contained in Appendix A.

2.4. Spectrometer

A Jarrell-Ash 15° Robin mount, 1-meter spectrometer (Model 78-751) was used to spectrally analyze the elastic scattering and fluorescence from the dye-filled capillary. The spectrometer employed a 1-meter radius of curvature concave diffraction grating with tripartate construction, an 80 x 40 mm ruled area with 590 grooves/mm, and a 2400 Å blaze wavelength at normal incidence. Independently adjustable entrance and exit slits controlled the light throughput and the spectral resolution.

The Model 78-751 belongs to the normal incidence class of off-Rowland circle spectrometers. Spectrometers of this type have a fixed angle between entrance and exit slits. The Robin mount has a 15° angle between between the slits to minimize astigmatism and polarization effects, and also to provide good accessibility to the slits.[19] Spectral scanning is accomplished by rotating the grating. During rotation, the grating moves linearly along the bisector of the angle subtended by the entrance and exit slits at the center of the concave grating. This movement controls focusing, while the grating rotation about a vertical axis tangent to its center produces the monochromatic effect.

A sine bar grating drive controlled movement of the grating. The drive had a four digit counter readout that was linear in wavelength. Wavelength scans from 0 to 7200 Å (first-order) were possible with a 12-speed reversible motor system. Scanning speeds from 1 to 5000 Å/minute were available. (The spectrometer's controls were originally specified for a 1180 groove/mm grating so the speed control settings and wavelength readout had to be multiplied by two.)

The first familiarization experiments produced spectral lines with distorted line shapes and full widths at half maximum intensity (FWHM) in excess of 5 Å. The irregularity of the spectral lines was due to improper focus alignment of the

tripartate grating. Each portion of a tripartate grating images light from the entrance slit (object plane) to the exit slit (image plane) separately. The slits and grating must be positioned such that the exit slit is at the common focus for each part of the grating. Otherwise, distorted line shapes occur.

Prescribed techniques for adjustment and alignment of the grating and slits[19,20] were followed to optimize the spectrometer focus. A mercury lamp with several strong, well-dispersed spectral lines in the visible region was used as the source during alignment procedures.

The grating was properly oriented with respect to its three mutually perpendicular axes first. Micrometer screws located on the grating mount allowed precise adjustment of the grating's rotation (vertical axis), tilt (horizontal axis in the plane of the grating), and level (horizontal axis normal to the grating plane). The grating was rotated about its vertical axis until the zero order image from the mercury source passed through the exit slit. Pieces of fine string were then placed horizontally across the vertical center of both slits. The tilt was adjusted so the zero order image of the entrance slit's string coincided with the string on the exit slit. Finally, the grating level was adjusted so the image and string coincided for the blue (4358 Å), green (5461 Å), and yellow (5770 Å) mercury lines.

The entrance and exit slit assemblies were then removed to repair the slit width adjustment mechanisms and clean the slit surfaces. Both slits were connected to the spectrometer by focusing tubes, which had screw devices for lateral focusing adjustment and slit rotation. Proper positioning of the entrance and exit slits was performed using the Foucalt method[19] to achieve the correct focus. The Foucalt method involves scanning each of the aforementioned wavelengths, viewing the illumination on the grating through the exit slit, and laterally positioning the slits with respect to the grating. Correct focus is achieved when the illumination on the

grating from the entrance slit appears and disappears uniformly across the entire grating, as opposed to its moving across the grating from side to side. After positioning, the entrance and exit slits were oriented parallel to each other and to the grating rulings for optimum spectral resolution. Parallel alignment is observed when the light from the incident scanned wavelength does not run from top to bottom or bottom to top across the grating, but illuminates the grating uniformly.

Figure 3 shows comparisons of line shapes before and after positioning/orientation of the grating and slit assemblies. Source, spectrometer, and photomultiplier tube parameters were identical for each figure. The resultant line shapes were sharper and had the FWHM reduced by a factor of approximately 14.

After completing the spectrometer's optical alignment, the entrance and exit slit assemblies were calibrated. Each slit had a micrometer dial which controlled the slit width (SW) separation between the slit jaws. The dials had divisional markings from 0 to 400 which nominally corresponded to the slit width in microns. The markings were readable to within one quarter of a division. Calibration of the entrance slit was accomplished by setting the exit slit to its maximum width and measuring the intensity of the mercury green line (5461 Å) for various entrance slit widths. The exit slit was calibrated in the same manner except the mercury source was attached to the exit slit and the photomultiplier detector was placed at the entrance slit. Intensity measurements were made for different exit slit widths while the entrance slit was kept open to its maximum width.

Figure 4 shows calibration curves for both slits in the regions where the dial mechanisms begin to open the slit jaws. The entrance slit jaws remained at a constant 1 micron separation for any dial setting below 202. As the dial was turned past 202, the entrance slit width in microns was given by the dial setting minus 201. The exit slit width was 1 micron when the dial setting was below 7.5

and equaled the dial setting minus 6.5 (in microns) for settings greater than 7.5. The aforementioned calibration relationships had an uncertainty of 1 micron, which was within the level of accuracy required for this experiment.

The maximum resolution that could be achieved with the spectrometer was next determined by measuring the FWHM as a function of entrance slit width for the mercury green line. With the exit slit maintained at a constant width (10 microns), the green mercury line was scanned in the forward and backward directions for progressively smaller entrance slit width settings while the corresponding line shapes were recorded for analysis. The minimum FWHM was 0.31 ± 0.04 Å and is illustrated in Figure 5. (The resolution specification in the spectrometer manual was 0.30 Å.)

The final adjustment and calibration performed on the spectrometer was for the sine bar wavelength drive. The drive consists of a threaded bar with a glass contact flat attached on one end which pushes against a grating pivot arm. A motor connected to a variable speed gear mechanism turns the threaded bar such that the grating pivot arm moves in or out, thereby moving the grating with respect to the fixed entrance and exit slits. The rotation of the threaded bar is linearly proportional to the wavelength so that the movement of the grating pivot arm is proportional to the sine of the diffraction grating angle. Accuracy of the wavelength drive depends on proper alignment of the glass contact flat angle with respect to the threaded bar and correct adjustment of the grating pivot arm length.

The wavelength counter was first corrected so the dial read zero for the peak of the zero order image from the mercury source. Next, wavelength error differences (wavelength counter reading - actual wavelength) for the blue, green, and yellow mercury lines were plotted versus their respective actual wavelengths to determine which adjustments were required. Measurements and adjustments were

made until a curve with the minimum wavelength error differences in the visible region was obtained. Wavelength error differences (Å) were improved from -18.6 to +0.48 for the blue line, from -12.5 to +0.02 for the green line, and from -26.4 to -0.06 for the yellow line. (A completely flat curve with zero error was neither attainable nor required for this experiment.)

After the final corrections to the drive were performed, a spectral line's wavelength in the visible region was given by approximately twice the wavelength dial reading. Although this approximation was adequate to identify well-dispersed spectral lines with known wavelengths, a more exact calibration was required to determine unknown spectral lines. Wavelength error differences were measured for several additional lines from the mercury source and a neon-iron hollow cathode source to establish a more accurate wavelength drive calibration. The resultant calibration equation, dispersion curve, and measured wavelengths (with wavelength differences in parentheses) in the wavelength region of interest are detailed in Figure 6.

A previously constructed wavelength trigger system relayed information to the data acquisition devices regarding the wavelength counter's position, and hence the position of the diffraction grating. Slight modification to the trigger system provided a square pulse output of variable voltage height and width each time the last digit of the wavelength counter was exactly zero or five. Both the chart recorder and computer A/D board allowed simultaneous acquisition of the intensity signal and wavelength pulses so extrapolation between pulses yielded precise information about the wavelength dial reading over any portion of a wavelength scan. These pulses were also used as triggers to begin and end data acquisition at specific wavelengths.

2.5. Photomultiplier Tube

An EMI Model 6256S photomultiplier (PM) tube was used as the detector. The PM employed a Spectrosil (fused silica) window, a 10 mm diameter Cs_3SbO photocathode, and 13 CsSb dynodes in a Venetian blind configuration which together had a peak quantum efficiency of approximately 21% at 4000 Å.[21] The maximum operating voltage was specified as -2200 V and the maximum anode signal current allowed was 100 microamperes. This tube was selected from several others because it had the best sensitivity in the blue-green spectral region and the lowest dark current.

The PM tube was mounted in a sealed base which was attached to the spectrometer's exit slit with a circular bracket. O-ring seals on both sides of the bracket prevented extraneous light from entering the spectrometer or PM tube. The base contained an internal 15-pin socket for the PM tube and two external BNC connectors for the applied negative voltage (cathode) and signal measurement (anode).

Dark current noise and signal to noise ratio for a constant intensity source had to be determined as functions of applied voltage in order to determine the optimal operating voltage. (The measured signal is not the true signal, but is actually the signal plus noise.) The measured intensity of the mercury green line with fixed slit widths (20 microns) was the signal. Both the dark current and signal were measured with a logarithmic picoammeter as the PM tube voltage was incremented in steps of -100 V from -1000 to -2100 V. Vacuum flap valves on both slit housings sealed off the PM tube from all light so the dark current could be measured at each voltage without affecting the mercury source. The PM output for any measurement was stable within one minute of any change in operating voltage or light flux incident on the cathode. The operating voltage which had the highest S/N ratio and the lowest error uncertainty was -1100 V (Figure 7), and was

therefore used for all experimental measurements.

2.6. Data Acquisition

Current measurement with a Keithley logarithmic picoammeter (Model 26000) was the primary method for signal detection from the PM. The picoammeter could measure current from 10^{-11} to 10^{-3} amperes with a corresponding 1 volt per decade recorder output from 0 to 8 V. A real-time record of the signal output voltage was provided by a two-pen Houston Instrument Series 4500 Microscribe strip chart recorder. Features of the chart recorder included 34 different chart speeds, 20 fixed voltage input voltage ranges with a variable span control to further adjust each range, and a digital display which provided a simultaneous readout of all operating parameters.

The microcomputer used for data acquisition was an Artisoft PC AT with an Intel 80286 CPU and 80287 Math Coprocessor. A Data Translation DT2801-A analog and digital input/output board provided the computer with the means for gathering the output voltage signal from the picoammeter. The A/D board had 12-bit resolution and was configured for eight differential input A/D channels (differential input channels have two switches per channel with one switch referenced to the analog common ground) and 0 to +10 V unipolar voltage input. A connector box was built with an RS 232 connector for the PC AT and BNC posts for each A/D channel input so signals could be readily applied. The software program used to interface between the input signals and A/D board was ASYSTANT+ from Asyst Software Technologies, Inc. ASYSTANT+ provided a comprehensive and flexible means for data acquistion, data processing, statistical analysis, and data file conversion for use in software plotting programs.

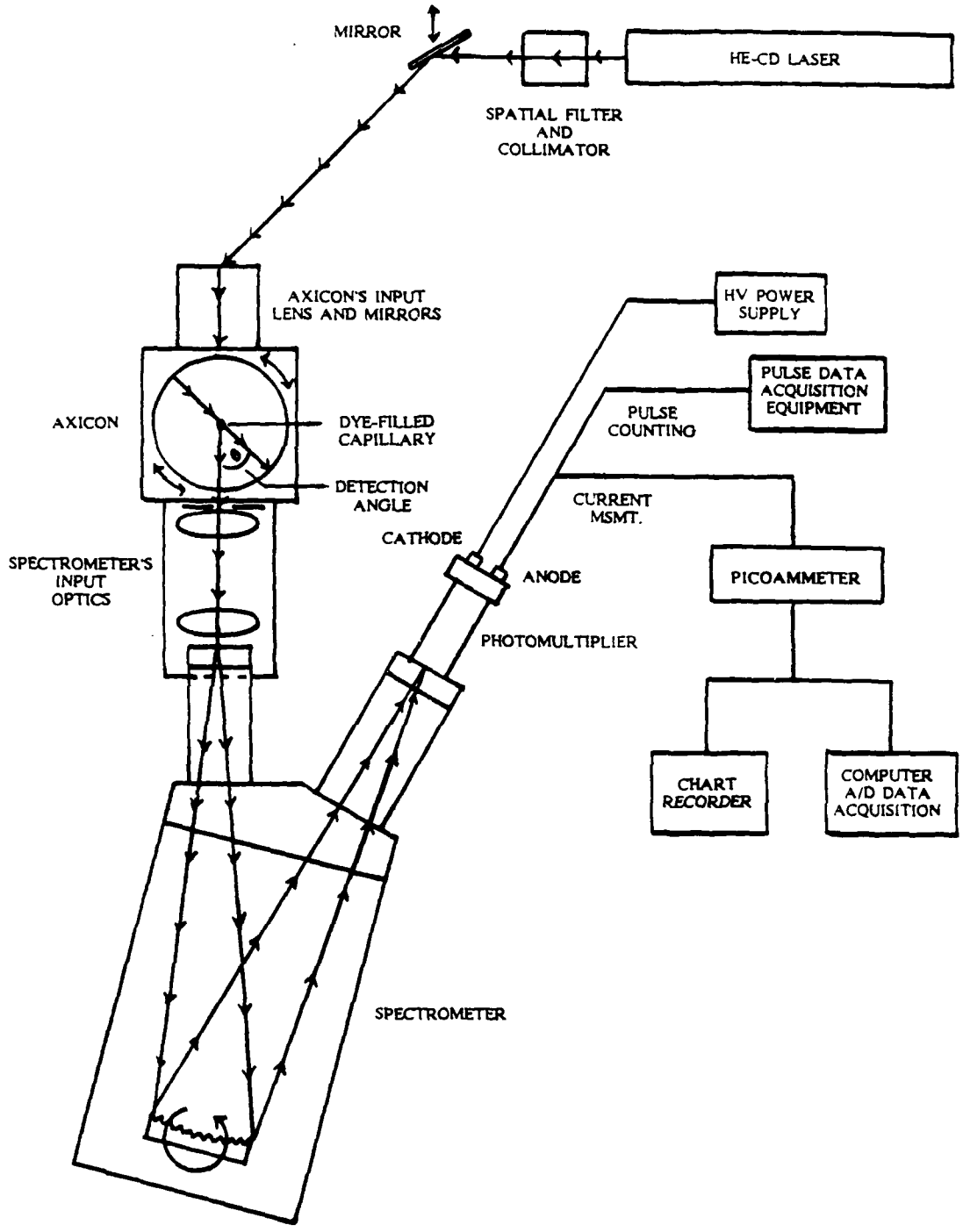

Figure 1. Diagram of the experimental system.

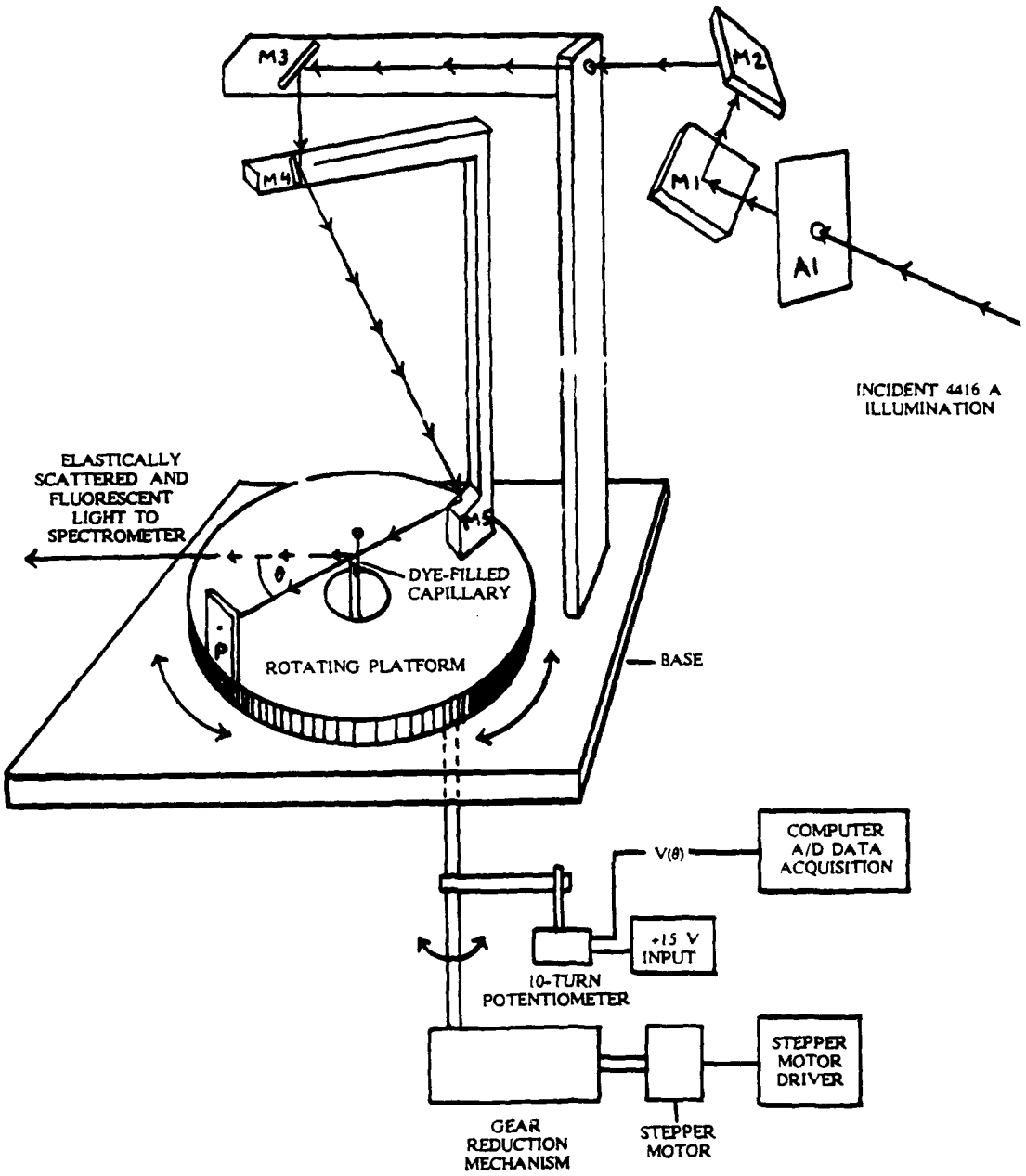

Figure 2. Diagram of the optical axicon.

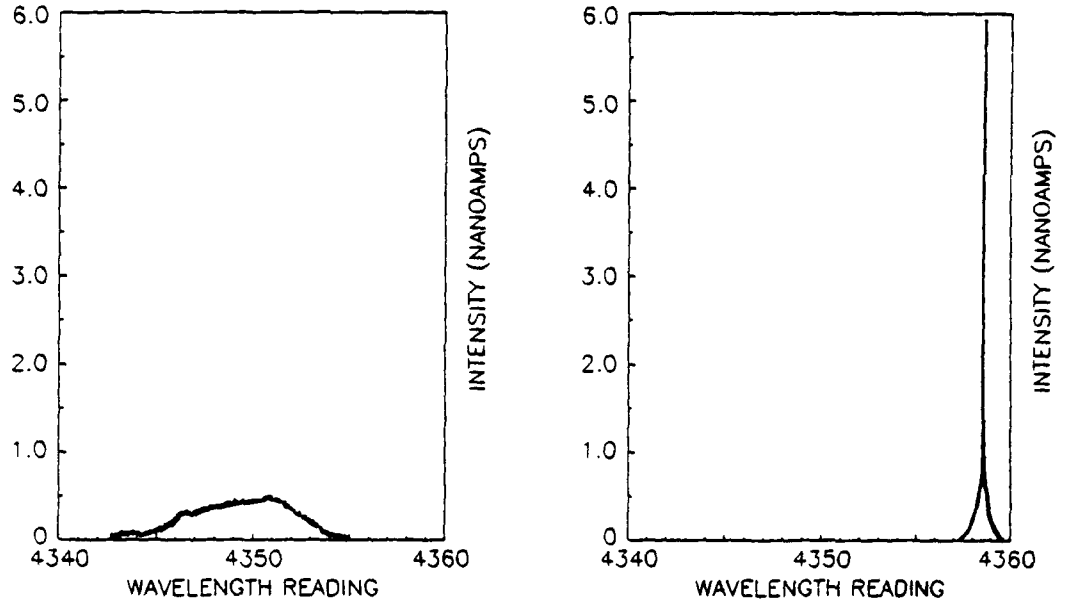

(A) Hg blue line (4358.34 Angstroms)

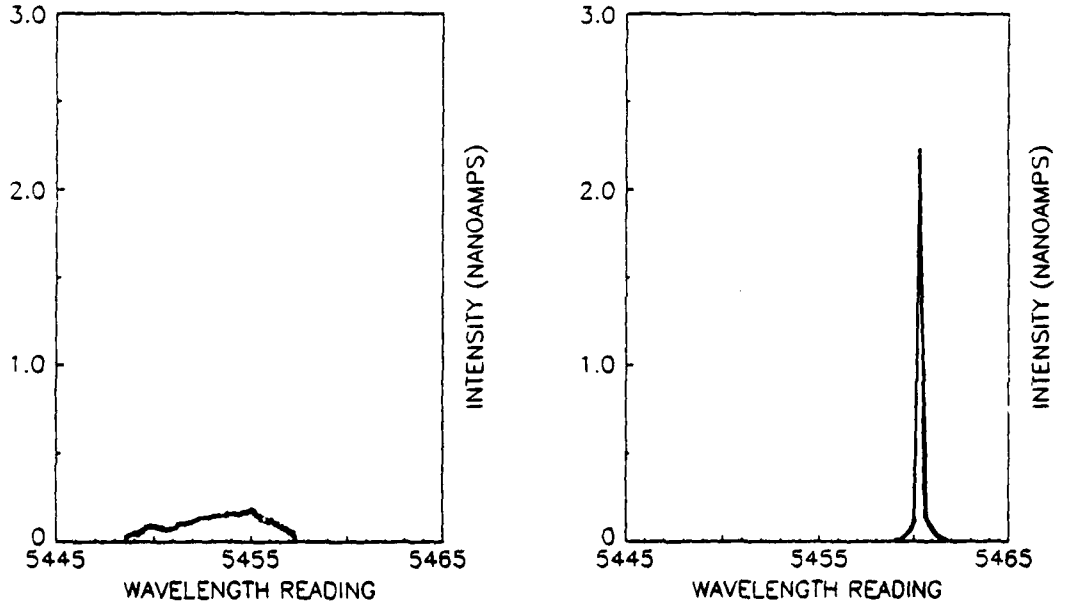

(B) Hg green line (5460.75 Angstroms)

Figure 3. Comparison of line shapes before (left side) and after (right side) spectrometer alignment.

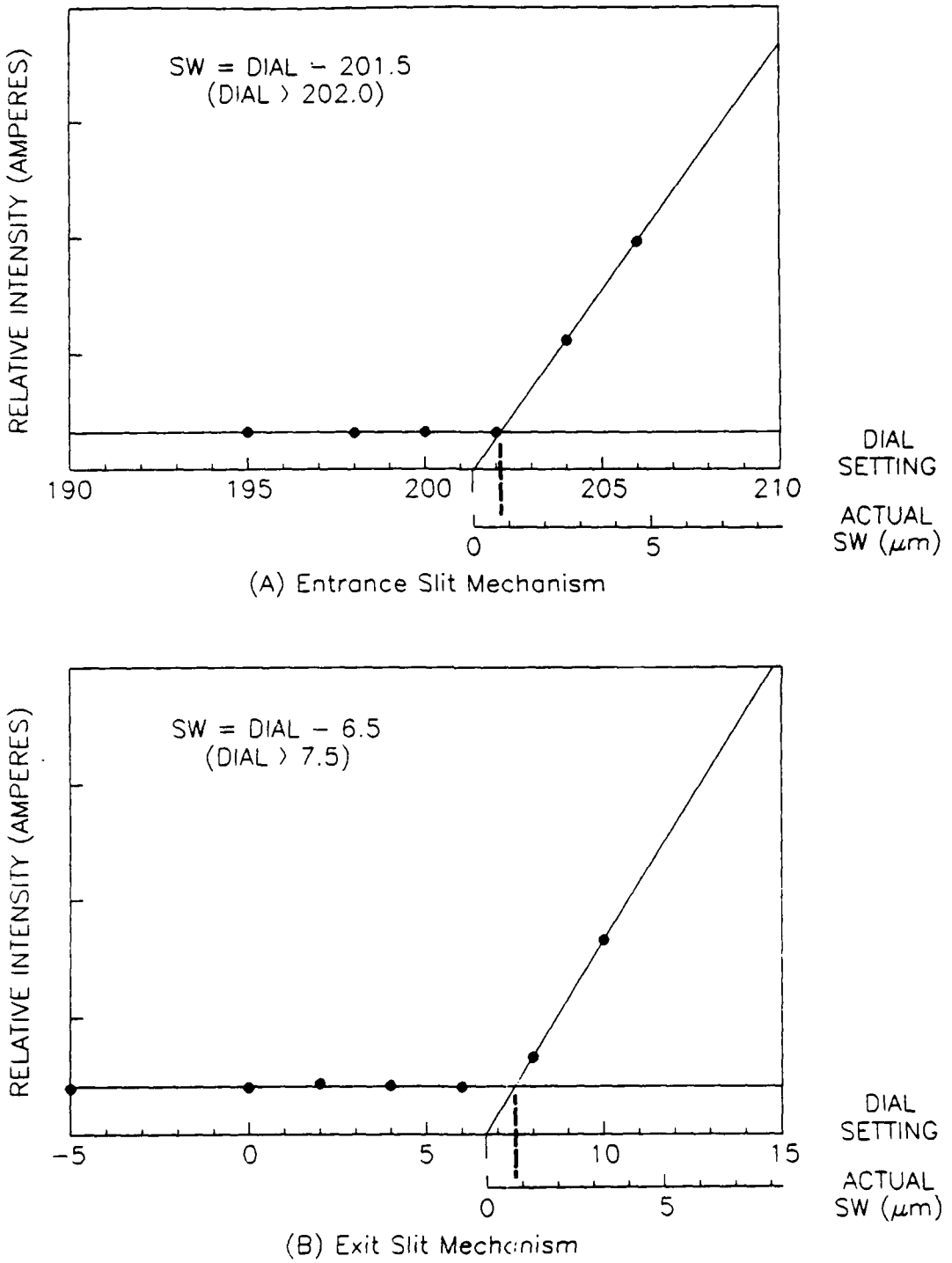

Figure 4. Spectrometer slit width calibration.
(Micrometer dials readable to within 1/4 division (0.5 μm).)

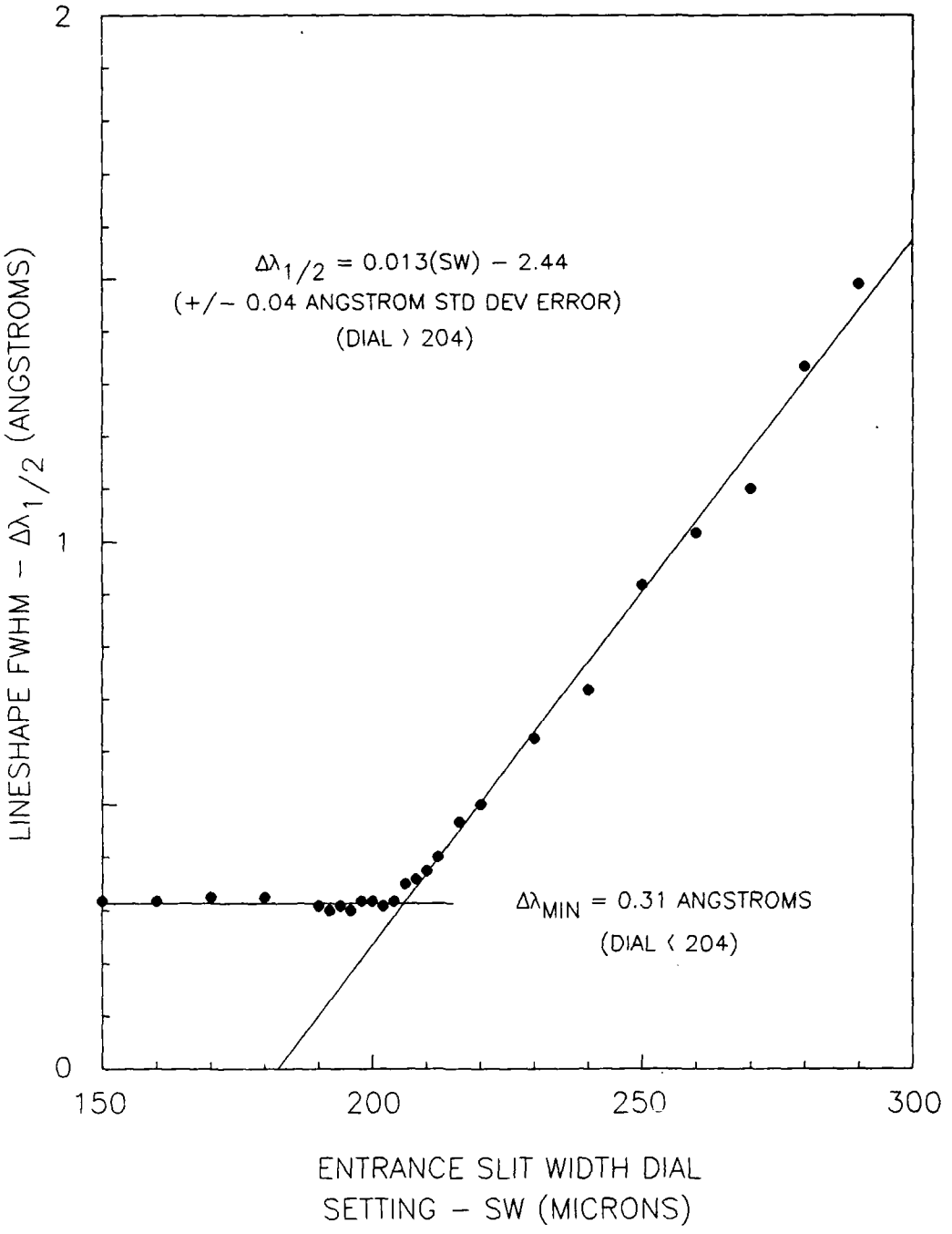

Figure 5. Line shape full width at half maximum intensity (FWHM) versus entrance slit width dial setting.

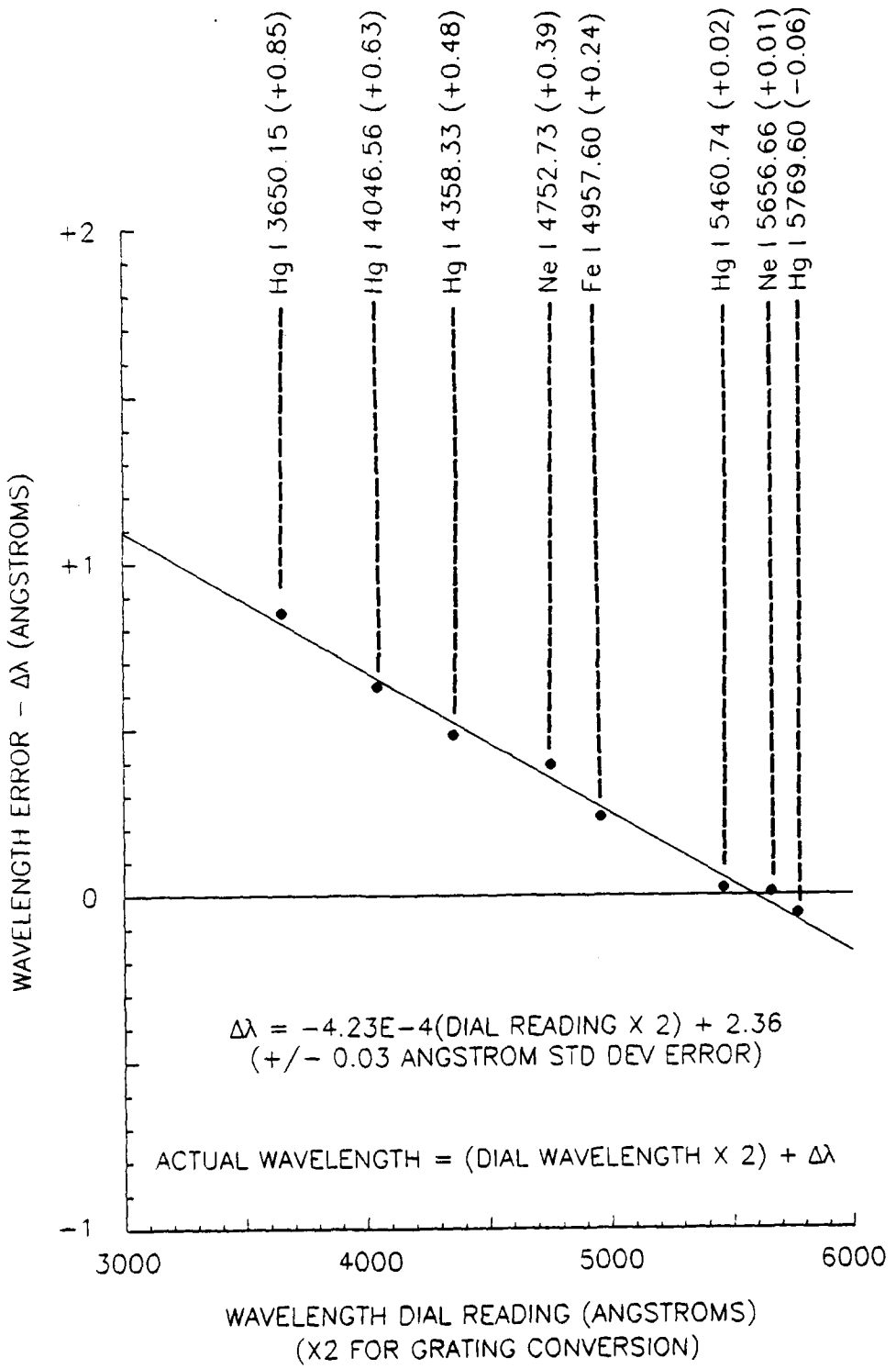

Figure 6. Wavelength drive calibration.

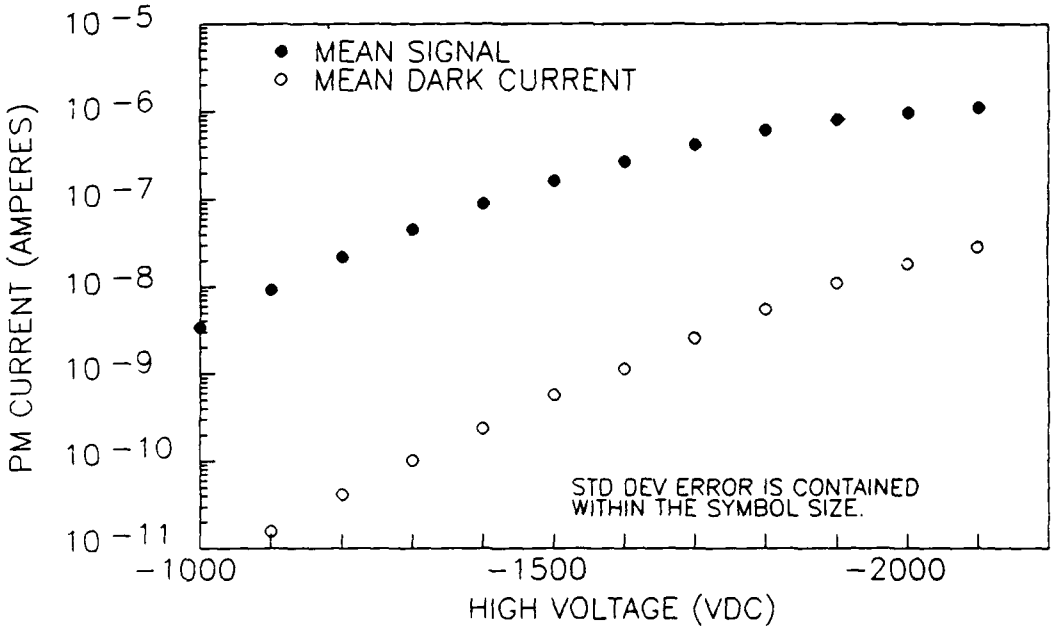

(A) PM Signal and Dark Current

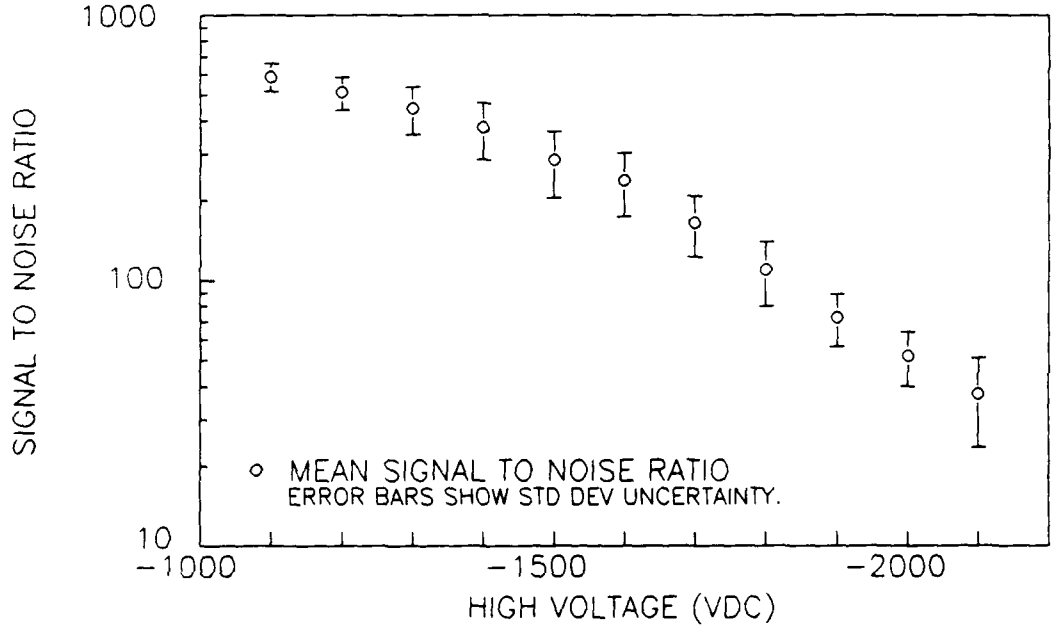

(B) PM Signal to Noise Ratio

Figure 7. Photomultiplier (PM) tube respons..

CHAPTER 3
THE EXPERIMENT

The elastic scattering and fluorescence from the dye-filled capillaries were studied in two different ways: as a function of wavelength at fixed detection angles and as a function of detection angle at fixed wavelengths. The nephelometer-spectrometer measurements were made without disturbing the dye-filled capillary's position and realigning the spectrometer's input optics. Three different capillary sizes were used to examine the emitted radiation: a 5000 micron (5mm) inner diameter "bulk sample test tube" and two smaller capillaries (1100 and 96.5 micron inner diameter). All were filled with fluorescent laser dye dissolved in ethanol.

3.1. Laser Dye

The fluorescent laser dye Coumarin 7 from Kodak was chosen for these experiments. It had characteristics similar to the organic materials used in CZE experiments, an absorption band maximum near the 4416 Å laser line, a high quantum efficiency of emitted fluorescence to incident illumination,[22] and minimal fluorescence degradation during extended excitation periods.[23] Use of Coumarin 7 in this type of research had been well-documented.[16] The chemical formula for Coumarin 7 (or Coumarin 535, dependent upon supplier) is 3-2'-Benzimidazolyl)-7-N, N-diethylaminocoumarin. The absorption band has a maximum near 4400 Å and the fluorescence band is primarily in the blue-green-yellow spectral region, ranging from approximately 4500 to 6000 Å. The two bands overlap roughly from 4500 to 5000 Å.

3.2. Sample Preparation

The Coumarin 7 laser dye powder was dissolved in ethanol (ethyl alcohol) at a concentration of 4 x 10^{-4} M. Previous research contributed to the decision for this specific dye-solvent mixture. Abromson's work showed Coumarin 7 had a higher solubility and the resultant mixture had a lower viscosity with ethanol than with several other solvents. Tuccio[24] had also demonstrated that 4 x 10^{-4} M was the optimum concentration to maximize the fluorescent signal for laser dyes dissolved in ethanol.

The 96.5 micron inner diameter sized-capillaries were cut from a large spool of Polymer Technologies hollow core fiber. The fiber had a fused silica (quartz) inner tubing and an opaque polymide outer coating (167 micron outer diameter), which distributed stress to prevent breakage of the quartz tubing. This fiber provided a uniform capillary geometry over the length of the sample, since the beginning and ending inner diameters of the fiber differed by only 1.3 microns over its 10 m length.

Short fiber sections were cut from the spool with an optical fiber cleaver. The sections were then passed through a candle flame to remove the flexible outer coating and provide a rigid quartz capillary. The capillary was placed in a small beaker containing the dye mixture and filled through capillary suction. Both ends were sealed with wax and the capillary was bonded to a specially-fabricated sample holder with a cyanoacrylate adhesive. The sample holders were made from brass rods and filed at one end to provide a flat surface for sample mounting.

Micro-hematocrit capillary tubes from VWR Scientific Inc., provided the 1100 micron inner diameter capillary. The tubes were made of type 2 glass, had a 1500 micron outer diameter, and no external coating. Other than removing the external coating, preparation of the 1100 micron inner diameter samples was the same as for

the 96.5 micron samples. A 5 mm inner diameter Kimble culture tube was used as the bulk sample container. It required only filling by an eyedropper and sealing of the open end.

3.3. Experimental Procedures

Placement of the dye-filled capillaries in the experimental setup is shown in Figure 8. A micro-positioning device was mounted below the base of the axicon to hold the sample holder with attached capillary. Sample holders were secured to the positioning device with a set screw. The center portion of the axicon's base and rotating platform were open so that the capillary could be supported from beneath with no side obstructions.

The positioning device had x-y translation, x-y tilt, and vertical adjustments to center the capillaries in the laser beam and orient the capillaries perpendicularly with respect to the beam. A capillary was determined to be centered in the incident beam when the elastic scattering was symmetric about the $\theta = 0^{\circ}$ and $\theta = 180^{\circ}$ directions. Normal beam illumination was accomplished by adjusting the capillary's tilt until the elastic scattering was in a plane perpendicular to the capillary and parallel to the axicon's base. Once the capillary was correctly positioned, the spectrometer's input optics were adjusted to maximize detection of the fluorescence. Repeated wavelength and/or angular scans could then be performed without further capillary or input optics adjustment.

The detection angle is the included angle between the paths of the incident laser beam and the direction from the capillary to the spectrometer's input optics (Figure 1). By convention, the forward direction ($\theta = 0^{\circ}$) is defined as the direction wherein the incident beam propagates straight into the spectrometer's input optics. The detection angle increases clockwise through the sidescatter region (approximately

$\theta = 90^{\circ}$) to the backscatter direction ($\theta = 180^{\circ}$), where the beam is directed exactly away from the input optics. Continuing clockwise, the angle increases through the opposite sidescatter region (approximately $\theta = 270^{\circ}$) until the forward direction is again reached ($\theta = 0^{\circ} = 360^{\circ}$). (The term "direction" refers to a specific detection angle, whereas "region" refers to a general angular range about a specific detection angle.) If the capillary is perfect and the system is accurately aligned, the scattered intensity should be symmetric about $\theta = 0^{\circ}$ and $\theta = 180^{\circ}$.

Angular scans were done at fixed wavelengths (4416, 4600, 4650, 4700, 4750, 4800, 4900, 5100, 5200, and 5500 Å) and wavelength scans were done at fixed angles (358°, 87°, and 176°) to study the 4416 Å elastic scattering and fluorescence from the different sizes of dye-filled capillaries. The wavelengths were chosen to concentrate primarily on the shorter wavelength portion of the fluorescence. Detection angles were chosen for several reasons: $\theta = 358^{\circ}$ ($\sim 0^{\circ}$) for the forward direction angle because the 4416 Å intensity was roughly two orders of magnitude lower than at $\theta = 0^{\circ}$; $\theta = 178^{\circ}$ ($\sim 180^{\circ}$) for the backscatter direction, since the axicon had a blocked region from approximately 177° to 183°; and $\theta = 87^{\circ}$ ($\sim 90^{\circ}$) for the sidescatter direction, because it was halfway between the forward scatter and backscatter angles.

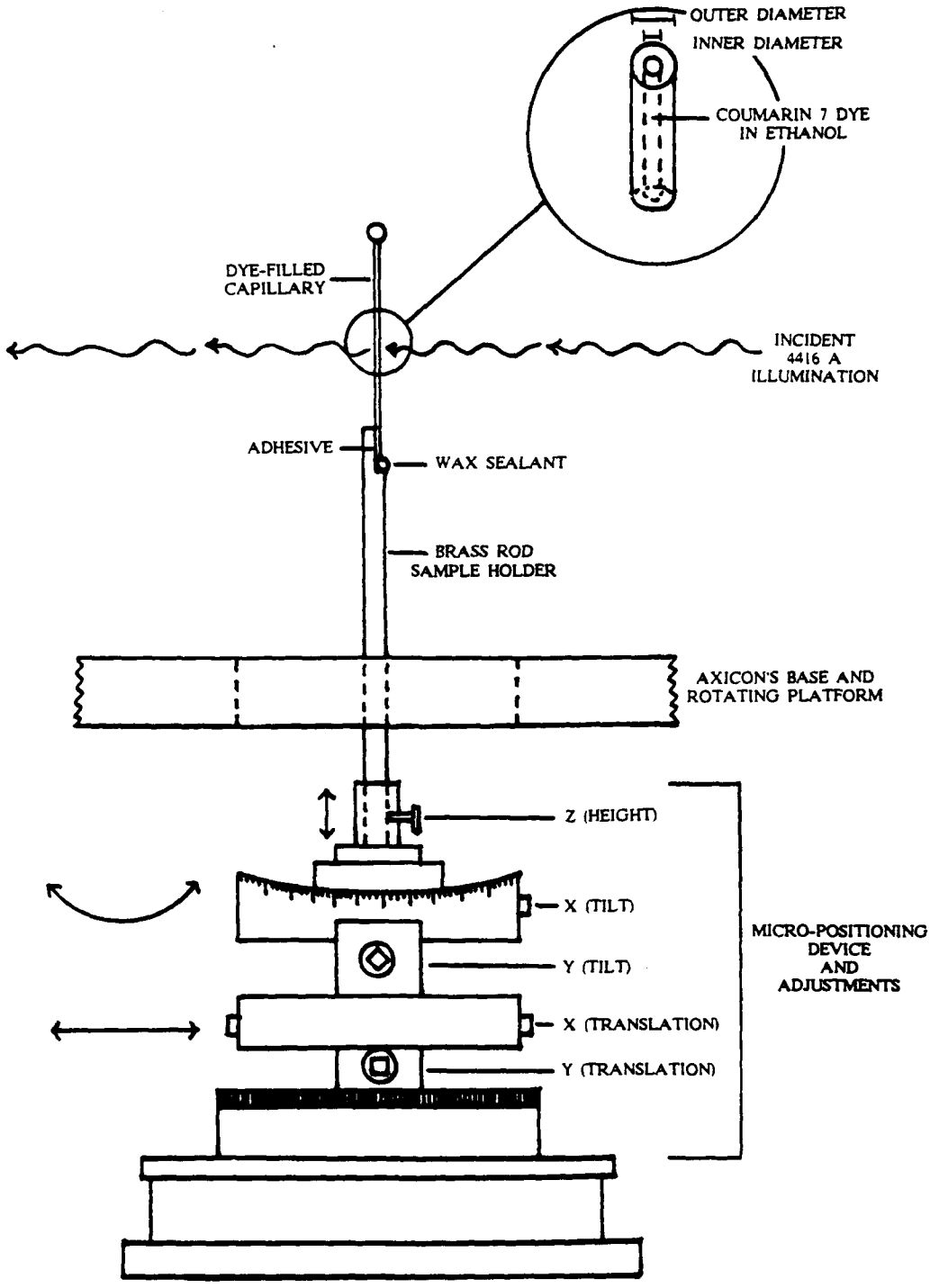

Figure 8. Dye-filled capillary mounted in the micro-positioning device.

CHAPTER 4

MODEL FOR FLUORESCENCE FROM HOLLOW CORE CAPILLARIES

The fluorescence from dye-filled capillaries can show angular differences for two reasons: the absorptive characteristics of the hollow-core material, and cavity resonances, which are setup inside the capillary. This work examined the effects associated with absorption in larger-sized capillaries. It was done in conjunction with Abromson's work to study smaller-sized capillaries where fluorescence enhancements due to cavity resonances are stronger.

If one looks at a fundamental system of a hot wire or tungsten filament heated by an electric current that emits radiation, no *wavelength, or intensity* differences are expected at different detection angles θ (viewed perpendicularly to the wire). Since the current heats the wire uniformly, the radiation can be said to truly originate uniformly over the surface of the wire. However, a wire that is heated by a beam of radiation (electrons, photons, etc.) normal to the wire's length could show angular differences in the emitted radiation. The back portion of the wire, which is directly illuminated by the incident radiation, becomes hotter than the front portion of the wire, and its radiation peaks in intensity at a shorter wavelength than that from the front portion due to this temperature gradient. As the diameter of the wire becomes smaller, the temperature gradient also becomes smaller and the emitted radiation differences between the front and back portions should become smaller. Since the wire cannot be made infinitely narrow, some finite temperature gradient will always exist. The emitted radiation from the front and back would then still be different though they might not be detectable.

The wire model with normal incident radiation helps explain the fluorescence from hollow core capillaries. Figure 9 shows an illustration of a dye-filled capillary illuminated with a 4416 Å laser beam. As the 4416 Å photons pass through a given volume in the capillary, dye molecules absorb the photons throughout that volume, become excited, and emit photons with longer wavelengths (less energy) in all directions. The 4416 Å intensity decreases as it goes through the capillary according to the exponential law of absorption, $I = I_o e^{-\alpha x}$, where the absorption coefficient α is the sum of the dye solution's absorption coefficient α_a, and a scattering coefficient α_s for scattered light which is removed from the incident beam. Figure 9 shows that fewer 4416 Å photons are available for absorption in a volume element at the front of the capillary than in a volume element at the back of the capillary due to the decrease in intensity. Fewer 4416 Å photons are therefore absorbed in the front volume element and less fluorescence is produced.

It is generally assumed that each volume element in the incident beam path fluoresces isotropically in all directions. The emitted wavelengths are spaced so closely together that the fluorescence spectra is essentially continuous. Since the dye's absorption and fluorescence bands overlap, the shorter fluorescent wavelengths, which are in this region of overlap, will themselves be absorbed by the dye.

The shorter wavelengths emitted by the strongly excited back volume element will be more intense in the backscatter direction, because they pass through fewer dye molecules in that direction, and experience less absorption. The shorter wavelengths radiated from the back volume element in the sidescatter and forward scatter directions must pass through more dye molecules and undergo more absorption. The contribution to the fluorescence at shorter wavelengths from this back volume element is therefore greatest in the backscatter direction and gradually

decreases toward the front scatter direction.

The front volume element also emits isotropically and its contribution to the fluorescence at shorter wavelengths is opposite that of the back volume element. It's greatest shorter wavelength contribution is in the forward scatter direction and gradually decreases toward the backscatter direction. However, the front volume element's contribution in the forward scatter is less than the back volume element's contribution in the backscatter because it is not as strongly excited as the back volume element due to the decreased 4416 Å intensity. Fewer shorter wavelength photons are emitted from the front volume element since fewer 4416 Å photons are available for absorption. Shorter wavelengths in the fluorescence should therefore be more intense in the backscatter direction than in the forward scatter direction. As the inner diameter size of the capillary decreases, the differences between the forward scatter and backscatter fluorescence decrease, but still exist because the capillary has a finite width.

When the incident beam diameter is smaller than the capillary inner diameter, dye molecules lying outside the beam path in the sidescatter directions are not excited by the 4416 Å illumination. However, fluorescent wavelengths emitted in these directions will undergo severe absorption by the unexcited dye molecules causing sidescatter intensity that is lower than the intensity in either the forward scatter or backscatter directions. As the capillary inner diameter becomes approximately equal to or smaller than the beam diameter, the entire core volume becomes excited, and the sidescatter intensity should approach the intensity in the other directions.

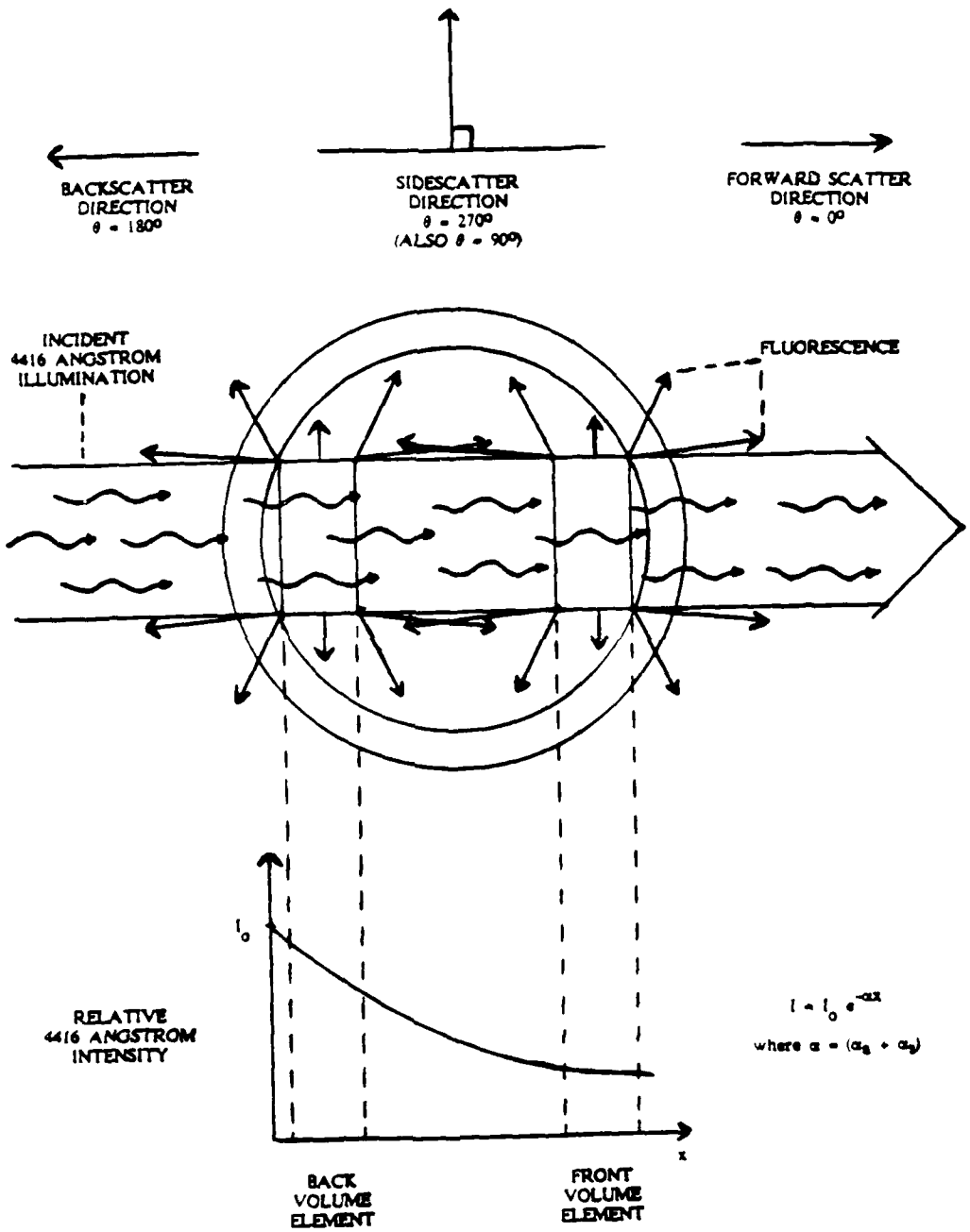

Figure 9. Diagram of fluorescence from dye–filled capillaries.

CHAPTER 5

RESULTS AND DISCUSSION

The initial signal measurements with the nephelometer-spectrometer setup examined the 4416 Å laser light throughout the entire wavelength region of interest (4300-6400 Å). The laser should create spectroscopic signals only at diffracted orders of the 4416 Å wavelength since it is a monochromatic source. However, "signals" were observed at all spectrometer wavelength settings due to spurious scattering and grating ghosts. These effects are shown and explained in greater detail in Appendix B.

This omnipresent 4416 Å signal overlapped the laser dye's fluorescence and was extraneous noise. The intensity of this noise, which varied with detection angle and wavelength, ranged from "zero" (the photomultiplier dark current level) to more than several orders of magnitude greater than the fluorescence from the excited dye. Bandpass interference filters with center wavelengths of 4416, 4900, 5100, and 5200 Å were used to separate the fluorescence from the 4416 Å background noise in those regions.

In order to establish an elastic scattering baseline and understand the scattering from the dye-filled absorbing capillaries, the elastic scattering from nonabsorbing empty and pure ethanol inner cores was studied for each capillary size using the techniques described earlier. Figure 10 shows the light scattered from the different core materials in 1100 micron inner diameter capillaries over the entire angular scanning region (θ = 0-360°). The intensity scale is logarithmic and shows details which would not be noticeable with a linear scale.

Although the elastic scattering for the three core materials have the same general form as expected, they differ in three important ways. First, the angular width of the forward scatter intensity peak at 0° is much narrower for the dye-filled capillary than for the other two core materials. Second, the dye-filled capillary's scattering in the backscatter region falls off more rapidly than the other core materials on either side of 180°. Third, the scattering from any of the three core materials is not exactly symmetrical about either the forward or backscatter directions. The most notable asymmetries are the unequal small peaks near 300° and 60° for the empty capillary; the sharp, half order of magnitude dropoff near 40° compared to the smooth curve at 320° for the capillaries with ethanol and Coumarin 7; and the unevenness of each curve about 180°.

Differences in both the forward and backscatter regions are primarily due to the absorptive characteristics of the material inside the hollow capillary. The empty and ethanol-filled capillaries do not significantly absorb the incident 4416 Å illumination, and they are nearly perfect elastic scatterers. However, the dye does absorb a significant portion of the incident 4416 Å light and less light is therefore available for scattering.

The elastic scattering should be symmetric about $\theta = 0^{\circ}$ and $\theta = 180^{\circ}$ for a correctly aligned, uniformly illuminated, perfect cylinder. Our capillaries probably contain imperfections and may not be perfectly cylindrical. Some asymmetry could be caused by slight laser beam motion during mechanical movement of the axicon's rotating base, which contains the aiming mirrors. (If the position of the beam moves slightly throughout the 360° angular scan, the capillary will not always be exactly centered in the incident beam.) Scattering measurements of the different core materials in the 5000 and 96.5 micron inner diameter capillaries yielded similar results.

4416 Å scattering from the 5000, 1100, and 96.5 micron inner diameter dye-filled capillaries are shown together in Figure 11. The most notable observation is the relative increase in the forward scattering (F) region to the backscattering (B) region as the capillary inner diameter size decreases. The backscatter and sidescatter (S) regions are nearly equal for the 96.5 micron capillary. (Lines under the F, S, and B in Figure 9 correspond respectively to the forward scatter, sidescatter, and backscatter fixed detection angles used in the wavelength scans. They are shown as a cross-reference between the angle and wavelength scans.) Although the width of the peak in the $\theta = 0^{\circ}$ direction becomes narrower with decreasing size, the region, which is 60° on either side of the forward direction, increases significantly with respect to the sidescatter region. Asymmetries are also present in the scattering for each capillary size.

The ratio of the forward scatter to backscatter depends primarily on the relative size of the dye-filled capillary with respect to the cross-sectional area of the incident illumination. The 5000 micron bulk sample tube was larger than the 4000 micron (4 mm) laser beam cross-sectional diameter. In this case, reflection occurs across the entire diameter of the laser beam, and the entire beam also propagates through the dye in the forward direction. The 1100 micron capillary had an outer diameter of 1600 microns and was therefore smaller than the beam diameter. In this case, a smaller beam cross-sectional area underwent reflection, which resulted in a decrease in the backscatter intensity. Also, part of the beam passes in the forward direction without obstruction by the capillary. This causes a relative increase in the forward scatter intensity. For the 96.5 micron capillary, the outer diameter is much smaller than the beam diameter. Therefore, less of the beam is reflected in the backscatter direction and more of the beam is unattenuated in the forward direction.

The sidescatter intensity is related to the ratio of capillary outer diameter to laser beam diameter and internal reflections inside the hollow core. As the sizes of the capillary inner and outer diameters decrease with respect to the beam diameter, more of the capillary's outer walls are directly illuminated and there is less dye to absorb internal reflections. Therefore, the sidescatter intensity increases relative to the backscatter intensity.

Comparison of the elastic scattering for the two dye-filled 1100 micron capillaries in Figures 10 and 11 show that different asymmetries can occur for the same capillary when later repositioned in the experimental setup. (The two figures cannot be compared on an absolute scale, because different neutral density filters were used to reduce the incident 4416 Å intensity and the input optics were adjusted between measurements. However, the different scattering measurements within each figure were taken with identical operating parameters.)

Expanded sections of the elastic scattering for the two smaller-sized capillaries are shown in Figure 12. These expanded views show that the scattering contains distinct intensity oscillations that are not noise fluctuations. The scattering for the 96.5 micron capillary has a lower oscillation frequency and larger amplitude than for the 1100 micron capillary, which is expected from the Mie scattering theory. The figure also shows that the 4416 Å scattered intensity at a given angular direction can be changed by nearly an order of magnitude with only a 1° change in the detection angle.

Wavelength scans for the 5000 micron bulk sample tube are shown in Figure 13. Comparisons of the fluorescence from the forward scatter to the backscatter directions show that the detectable onset wavelength of the fluorescence shifts from approximately 4625 to 4475 Å, and the maximum intensity wavelength of the fluorescence shifts from approximately 4975 to 4900 Å.

Figure 14 shows angular scans for the 5000 micron tube at three fixed wavelengths. The wavelengths are marked for cross-reference to other figures as follows: 4600 Å represented by L (low end of the fluorescence); 4750 Å by M (midway up the fluorescence); and 4900 Å by H (high end or peak of the fluorescence). This figure shows the wavelength dependence on the detection angle. As the wavelength increases, the relative fluorescence in the forward region increases with respect to the backscatter region until the fluorescence is approximately equal in both regions. The sidescatter region's fluorescence, although also increasing for longer wavelengths, always remains less than that of both the forward and backscatter regions. This is expected when the beam diameter is less than the capillary's inner diameter.

The data from all the 5000 micron tube angular and wavelength scans are combined in Figure 15 to show the fluorescence as a function of both angle and wavelength. Interpolation between the actual data points in the three-dimensional figure clearly shows more intense shorter fluorescent wavelengths in the backscatter region.

Figures 16, 17, and 18 show a set of measurements for the 1100 micron dye-filled capillary similar to Figures 13, 14, and 15. The wavelength scans in Figure 16 show that the peak fluoresent wavelength does not shift as much as that from the 5000 micron tube. The wavelength region in the onset of the fluorescence is also obscured in the forward scatter and backscatter directions by the 4416 Å background noise. However, the slope of the shorter wavelength side of the fluorescence decreases from the forward to backscatter directions, which would indicate a corresponding decrease in the fluorescence onset wavelength. The 4416 Å background noise was subtracted from the angular scans in Figure 17, and this figure more clearly shows the angular fluorescence at the three fixed

wavelengths. The fluorescence is nearly equal across the entire angular scan at 4900 Å wih no degradation in the sidescatter region since the laser beam is larger than the capillary inner diameter. Figure 18 shows the wavelength and angular dependence of the fluorescence.

The 4416 Å background noise became a significant problem in fluorescence detection for the 96.5 micron inner diameter capillary. For the wavelength scans shown in Figure 19, the fluorescence in the forward scatter direction is almost completely overwhelmed by the 4416 Å background noise. At first glance, the sidescatter and backscatter scans show little difference between their respective fluorescence. The shorter wavelength portions are expanded in Figure 20 and do show a difference in the onset wavelength of the fluorescence. The fluorescence rises above the 4416 Å noise at approximately 4655 Å in the backscatter direction versus approximately 4690 Å in the sidescatter direction. Angular scans and the three-dimensional figure are not shown for the 96.5 micron inner diameter capillary because of the high 4416 Å noise level.

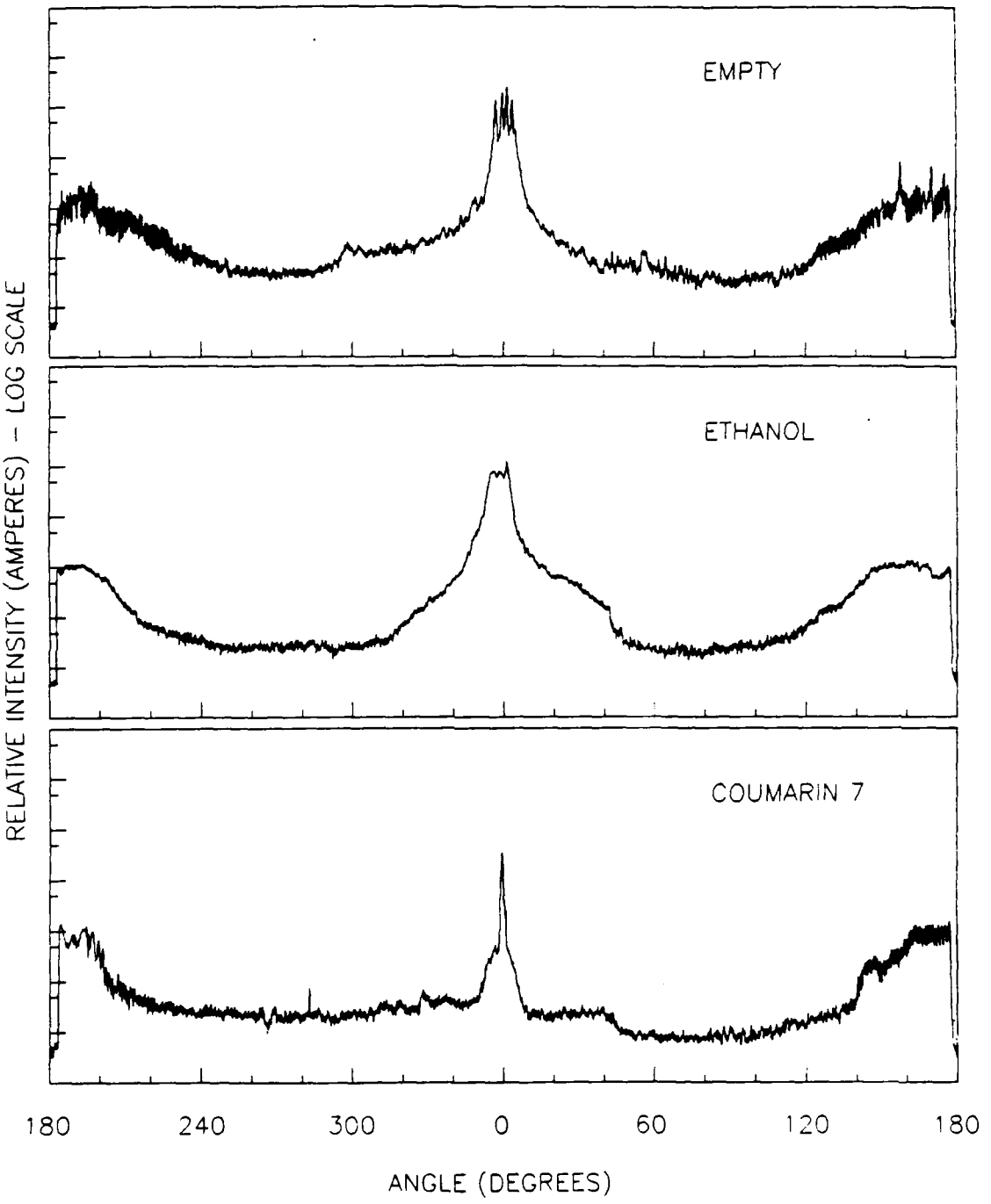

Figure 10. 4416 Angstrom scattering from an 1100 μm inner diameter capillary with different core materials.

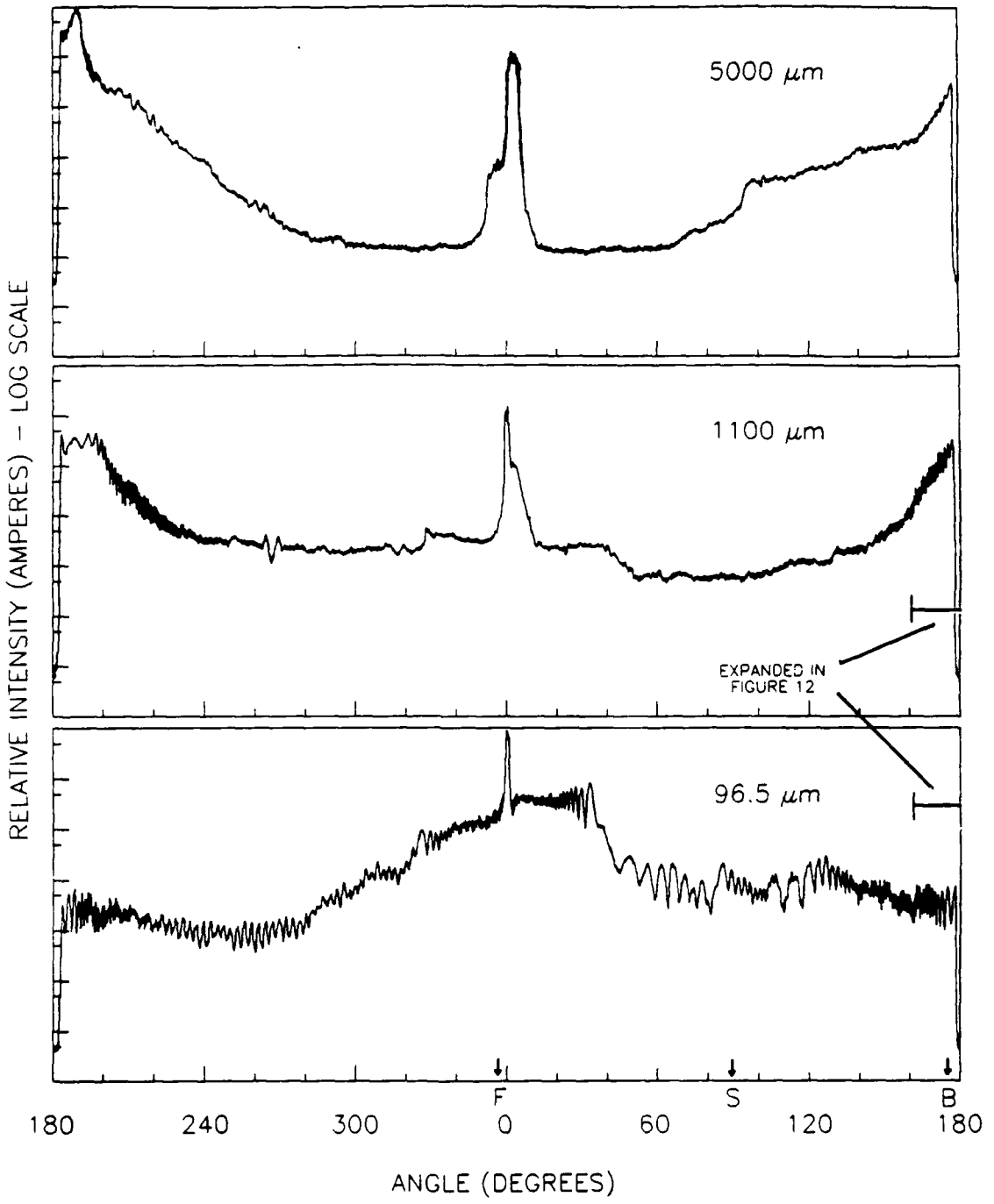

Figure 11. 4416 Angstrom scattering from the three inner diameter sizes of Coumarin 7–filled capillaries.

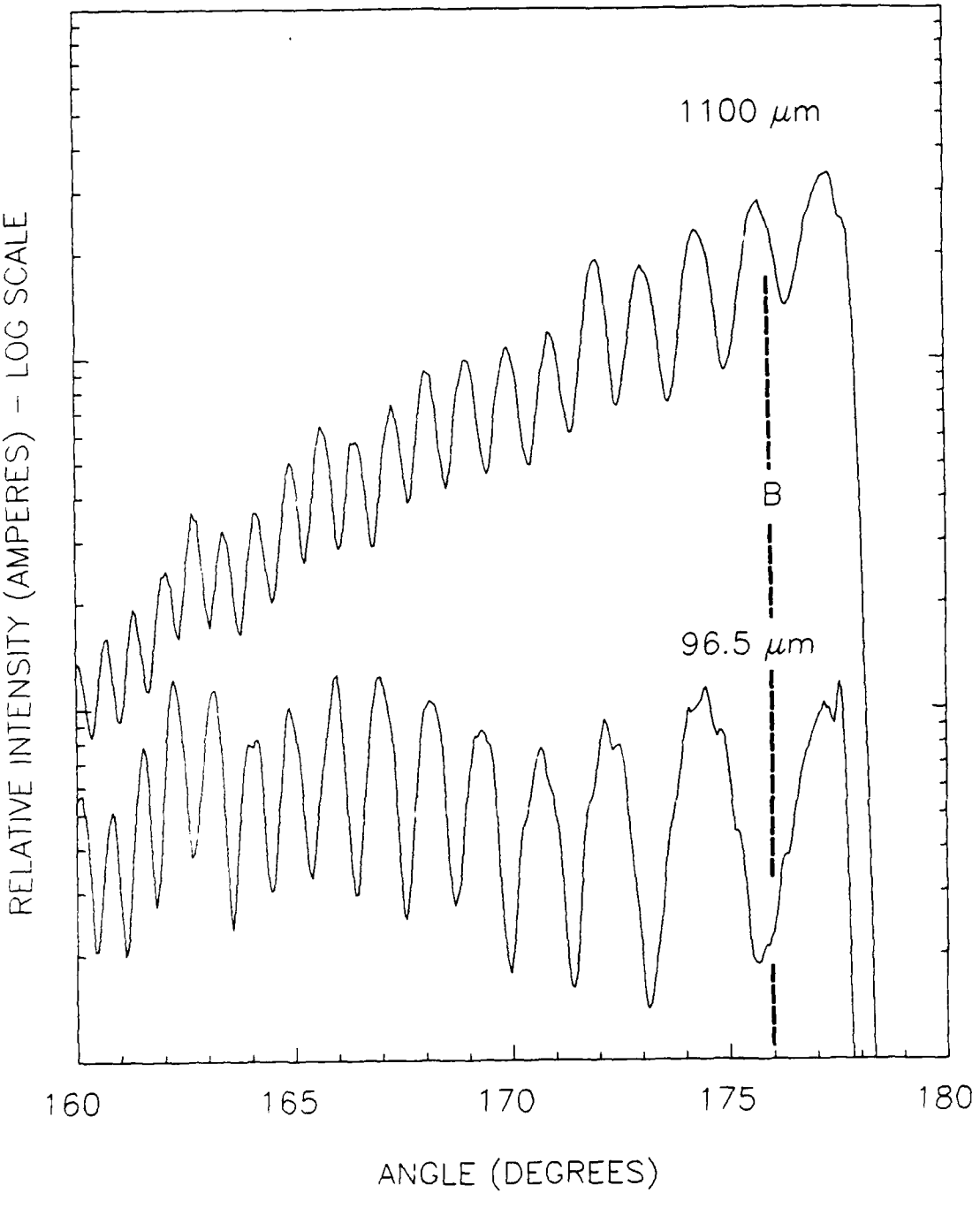

Figure 12. Expanded sections of 4416 Angstrom scattering from Figure 11.

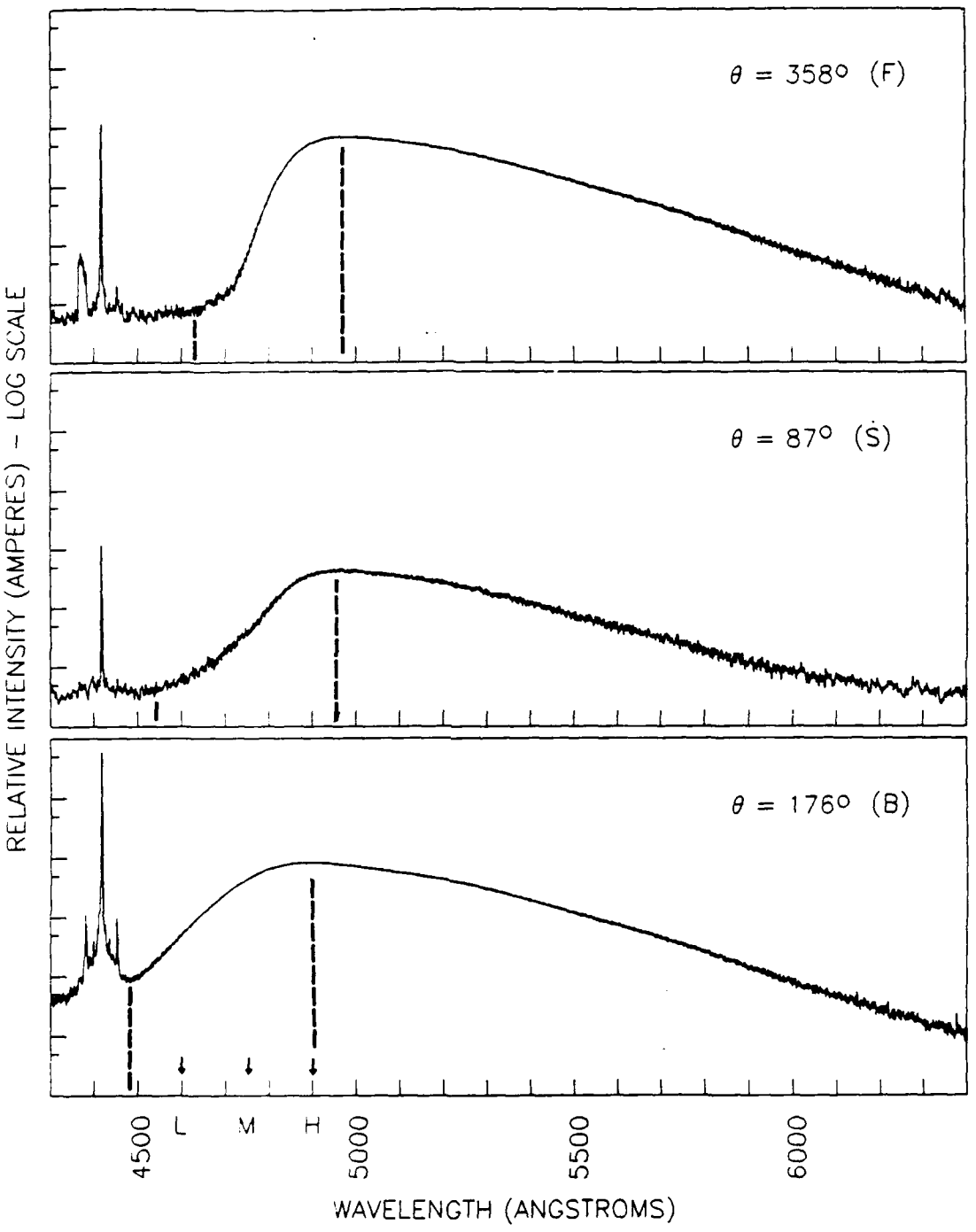

Figure 13. Wavelength scans of Coumarin 7 dye fluorescence from a 5000 μm inner diameter bulk sample tube.

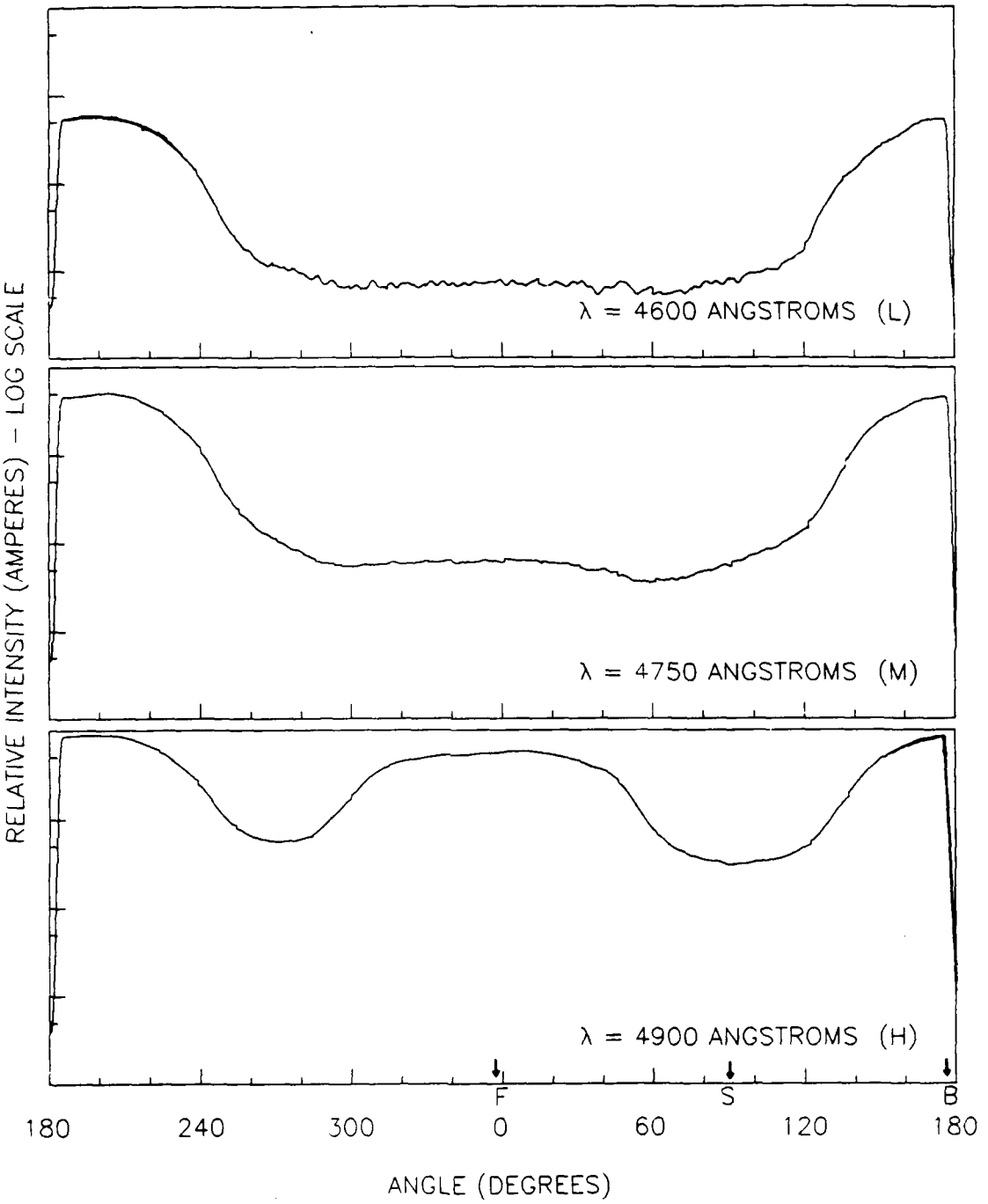

Figure 14. Angular scans of Coumarin 7 dye fluorescence from a 5000 μm inner diameter bulk sample tube.

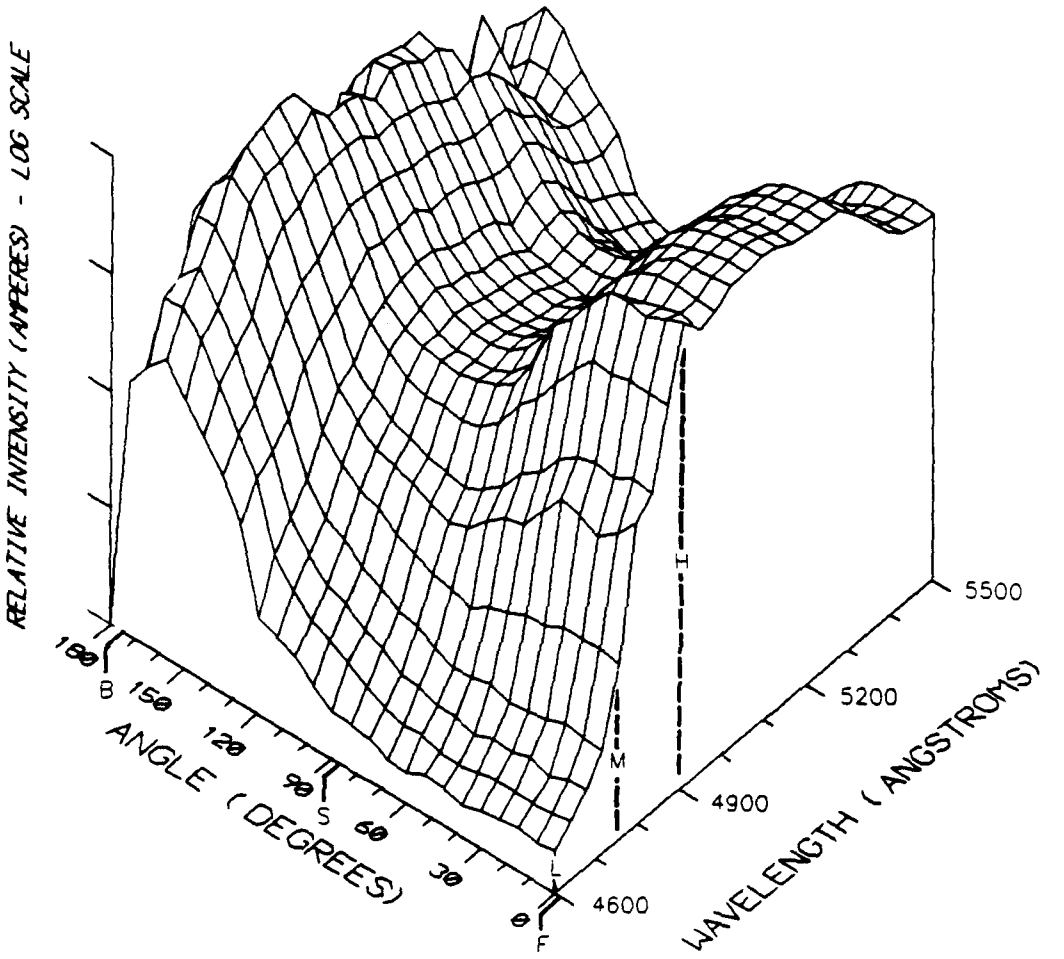

Figure 15. Fluorescence from the 5000 μm inner diameter bulk sample tube as a function of detection angle and wavelength.

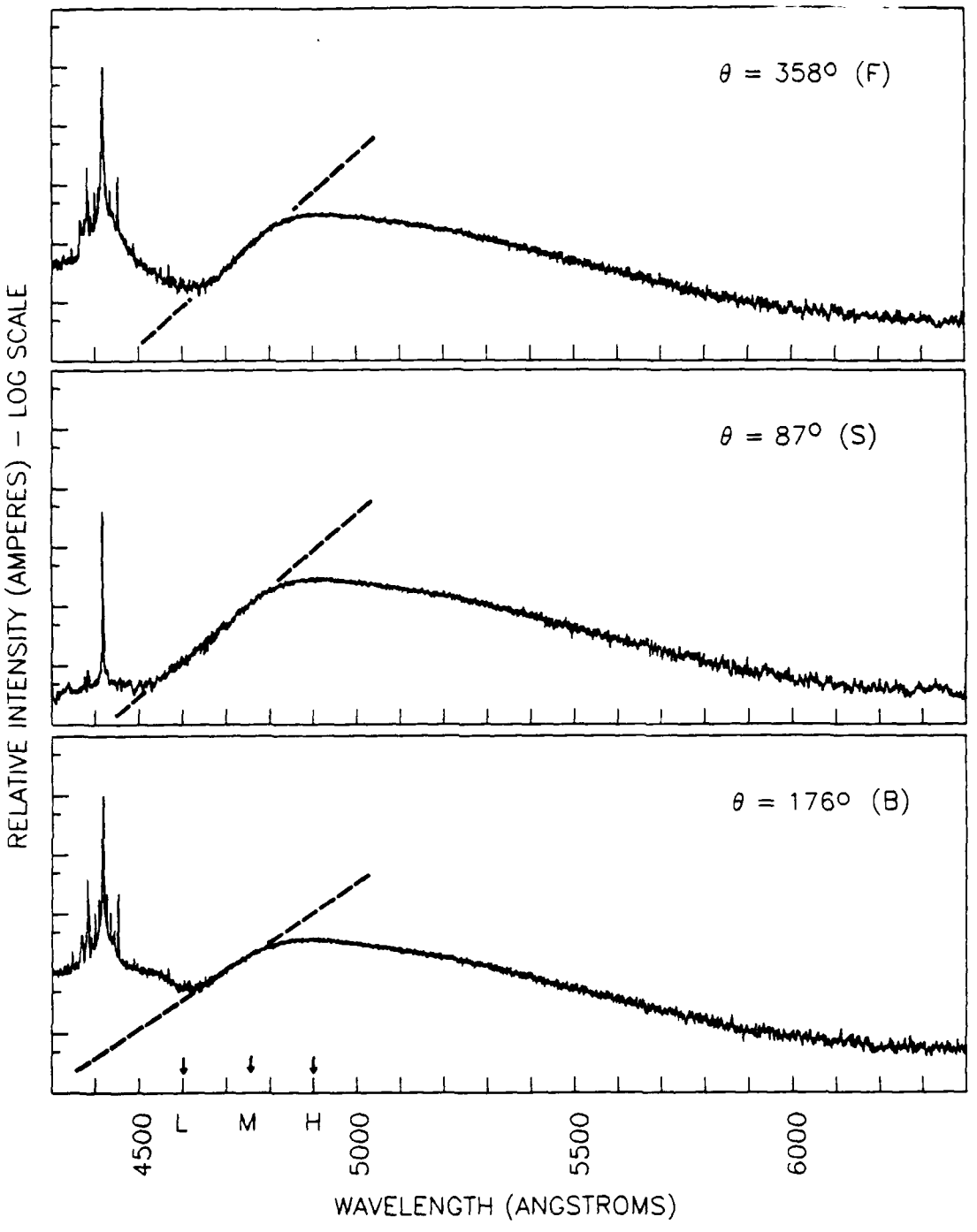

Figure 16. Wavelength scans of Coumarin 7 dye fluorescence from an 1100 μm inner diameter capillary.

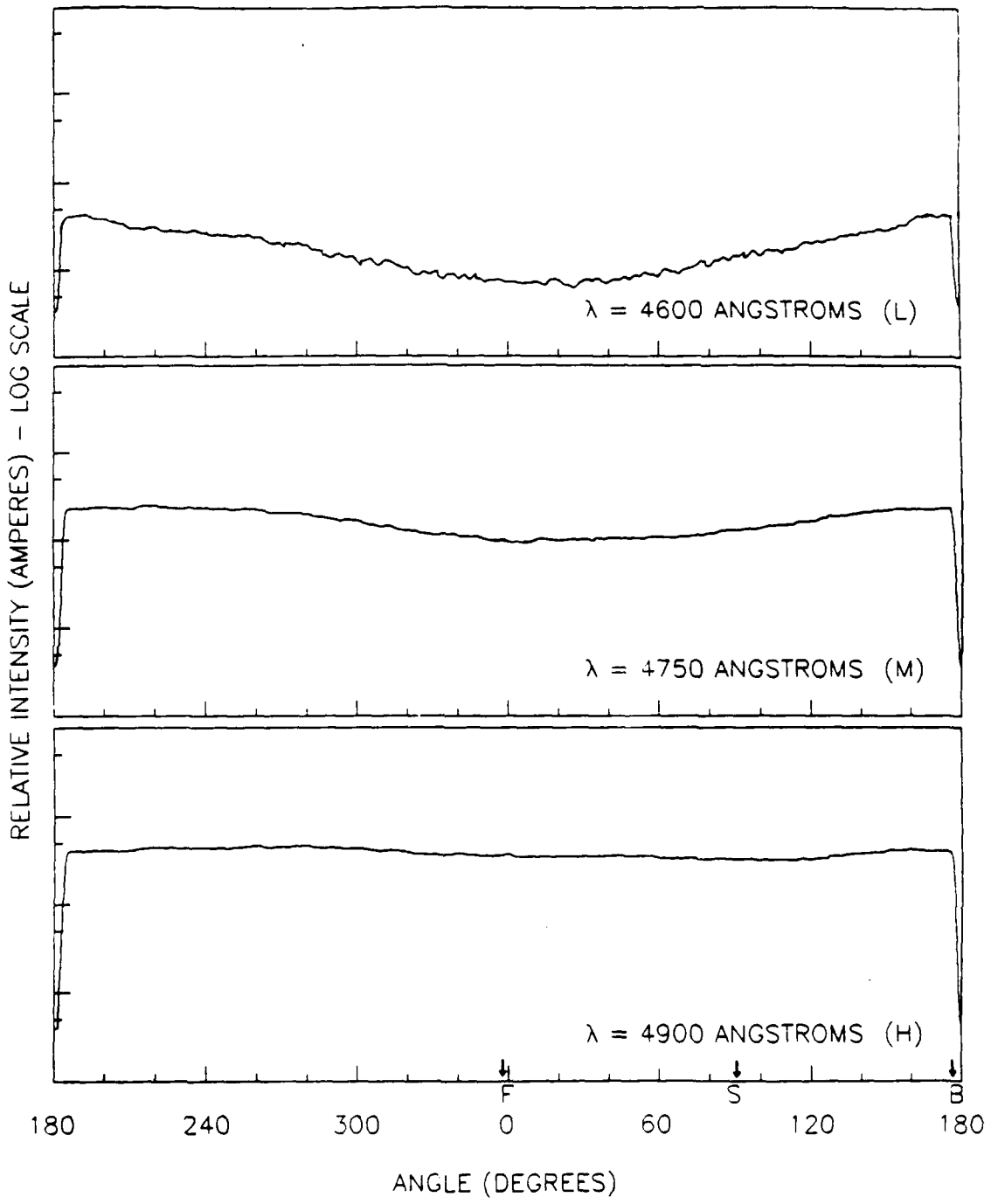

Figure17. Angular scans of Coumarin 7 dye fluorescence from an 1100 μm inner diameter capillary.

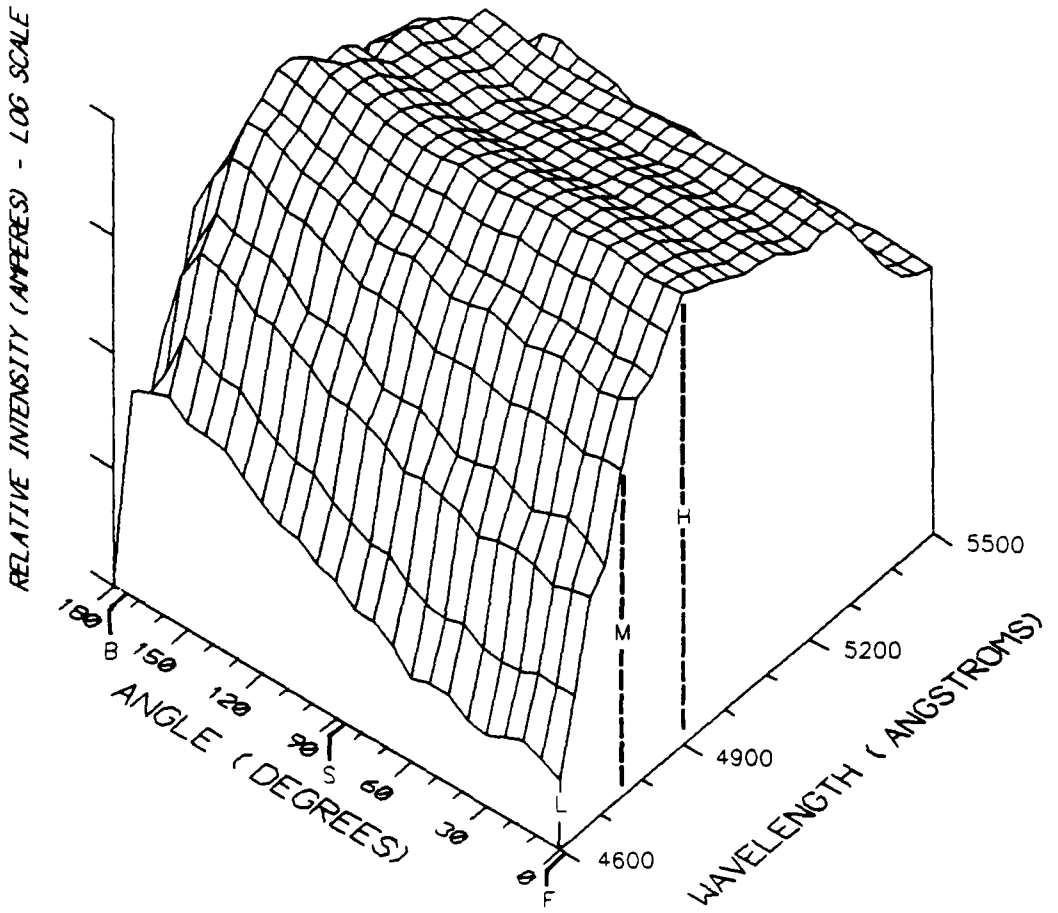

Figure 18. Fluorescence from the 1100 μm inner diameter capillary as a function of detection angle and wavelength.

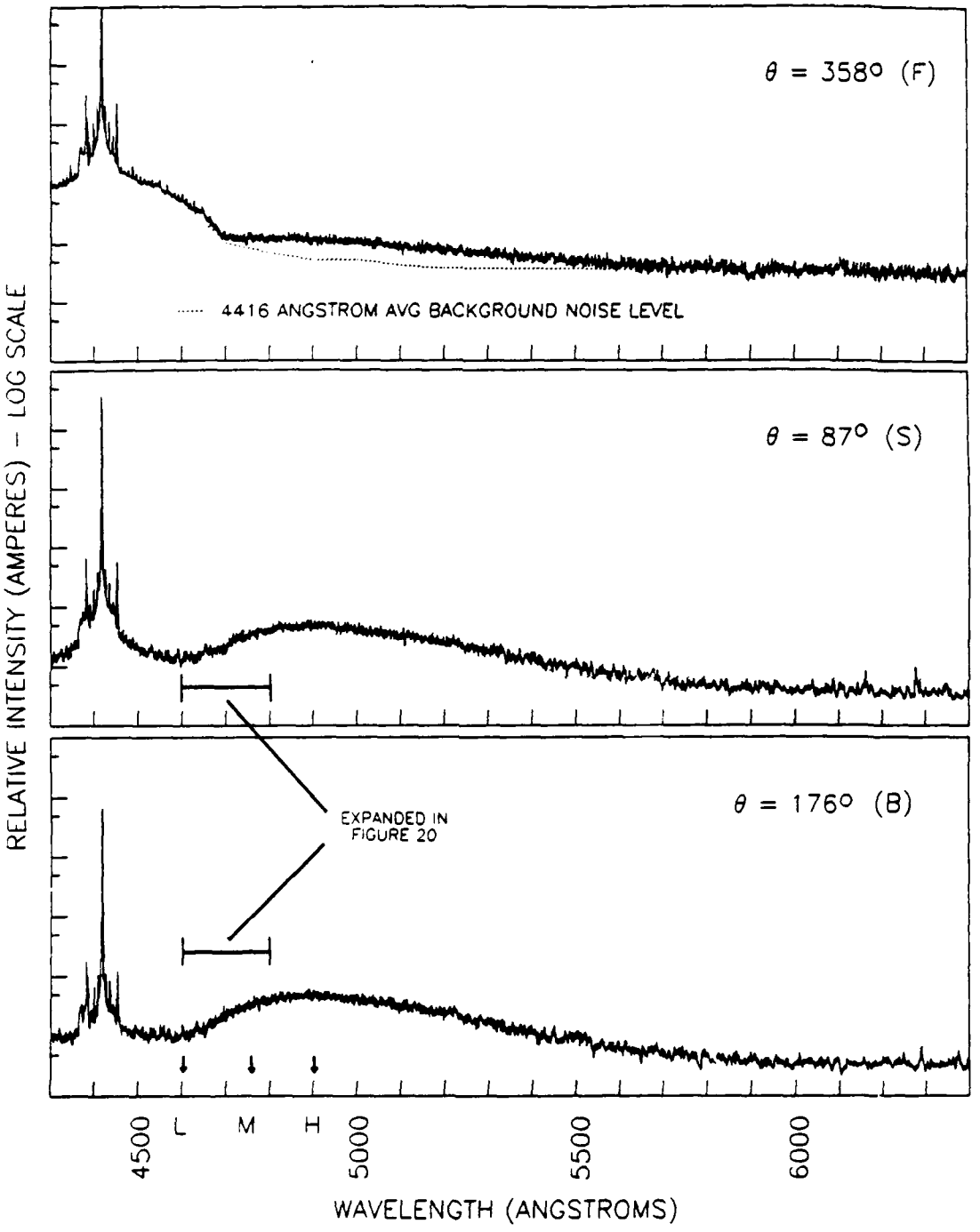

Figure 19. Wavelength scans of Coumarin 7 dye fluorescence from a 96.5 μm inner diameter capillary.

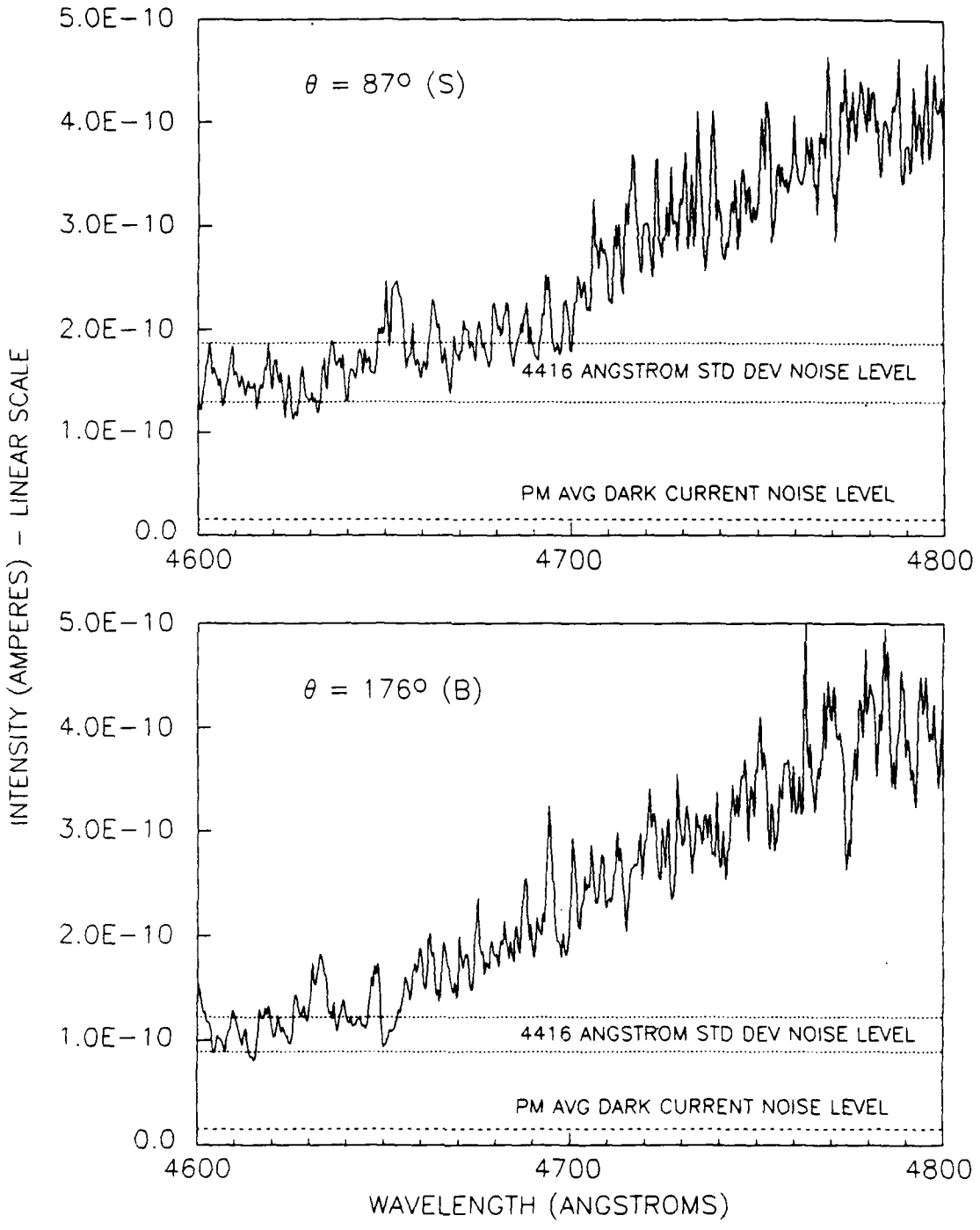

Figure 20. Expanded sections of 96.5 μm capillary wavelength scans from Figure 19.

CHAPTER 6

CONCLUSIONS

These experiments have confirmed an important hypothesis: the fluorescence emitted from small dye-filled capillaries is highly angular and wavelength dependent. Shorter wavelength fluorescence is more intense in the backscatter region than in either the forward or sidescatter regions. These angular forward to backscatter fluorescence differences decreased significantly as the capillary inner diameter size decreased, but were still measurable for the 96.5 micron capillary.

The 4416 Å excitation illumination elastically scattered from the capillaries, and contributed a substantial source of noise to the fluorescent signal. As the capillary size decreased to 96.5 microns, the scattered oscillation frequency decreased, and its amplitude increased. Amplitude variations changed by nearly an order of magnitude for an approximately 1° change in detection angle.

In real CZE experiments, where the fluorescence of biological materials is several orders of magnitude lower (less efficient) than laser dyes, higher power lasers are needed to create detectable fluorescent signals. In this case, the weak fluoresent spectra could be severely contaminated by the intense ubiquitous excitation illumination. The scattering and fluorescence characteristics of the sample-filled capillaries should be studied prior to CZE experiments, so that noise levels and optical artifacts can be discovered. This information could lead to an optimum detection angle that could reduce background noise and enhance the detection of certain wavelengths. As the capillary size gets smaller, the background noise could be reduced by much more than an order of magnitude. Although an

optimimized detection angle may provide only a slight advantage in signal detection, that advantage may be all that is needed when searching for weak signals from the small amounts of biological material studied in CZE experiments.

APPENDIX A

SPECTROMETER INPUT OPTICS

The spectrometer input optics were designed to fill the grating so loss of spectral resolution would not occur and to have a narrow "exit" optics angular width from the capillary so the angular fluorescence and scattering differences could be resolved. As the capillary inner diameter size decreases, the fluorescing core material begins to resemble a point source in the horizontal plane containing the optical axis. When a point source is far away from the spectrometer, the angular width of light transmitted through the spectrometer's entrance slit is narrow, but the grating is not filled. However, if the point source is moved close enough to the entrance slit to fill the grating, the angular width of light transmitted from that point source will be relatively large.

Figure A1 shows a ray trace diagram (top view) of the capillary, input optics, and spectrometer entrance slit and grating. First-order and thin lens approximations were used in the ray trace parameter calculations. The slit aperture and two achromatic lenses approximately fill the grating in the horizontal plane with an "exit" optics angle of 1.25° from the capillary.

A ray trace diagram in the vertical plane about the optical axis is shown in Figure A2. The ray trace parameters were calculated from the spectrometer back through the input optics, since the grating, and no longer the slit aperture, limited the transmission of light through the spectrometer. Chief ray parameters were scaled by the 4-mm-capillary height (2 mm above and below the optical axis), which is illuminated by the laser.

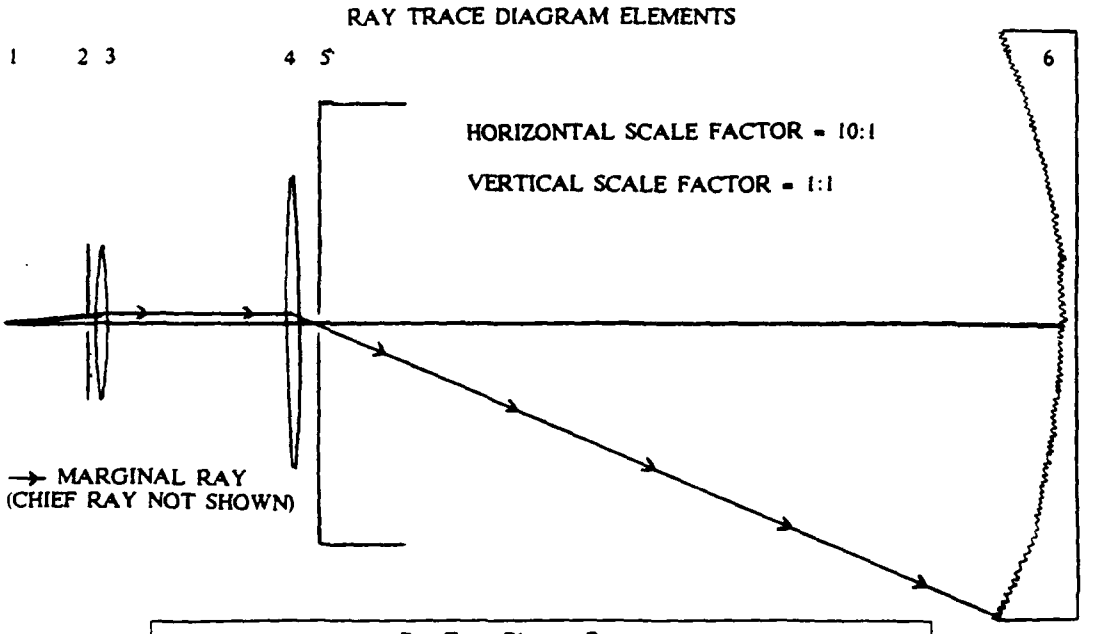

Ray Trace Diagram Parameters
(All lengths in millimeters; all angles in radians)

Element (Element #)	Physical dimension	Distance to next element	Focal length (power)	Marginal ray y-height w'-angle	Chief ray $\bar{y}$-height $\bar{w}'$-angle
Capillary (1)	D=9.65E-2 (design size)	115	NA	0 1.09E-2	4.83E-2 -4.20E-4
[Aperture Stop] Slit aperture (2)	W=2.5	11	NA	1.25 1.09E-2	0 -4.20E-4
Collimating lens (3)	D=20.5	265	126.0 (7.94E-3)	1.37 0	-4.62E-3 -3.83E-4
Focusing lens (4)	D=38.0	34.8	34.8 (2.87E-2)	1.37 -3.94E-2	-1.06E-1 2.67E-3
Entrance slit (5)	Variable	1000	NA	0 -3.94E-2	-1.33E-2 2.66E-3
Grating (6)	W=80	NA	1000	-39.4 —	2.65 —

"Exit" optics from capillary: $F/\# = -\frac{1}{2w_i'} = \frac{1}{2(1.09E\text{-}2)} = 45.9\ (1.25°)$

Input optics to spectrometer: $F/\# = -\frac{1}{2w_i'} = \frac{1}{2(3.94E\text{-}2)} = 12.7$

Spectrometer: $F/\# = \frac{f_s}{D_s} = \frac{1000}{80} = 12.5$

Figure A1. Ray trace diagram (top view) of the spectrometer input optics.

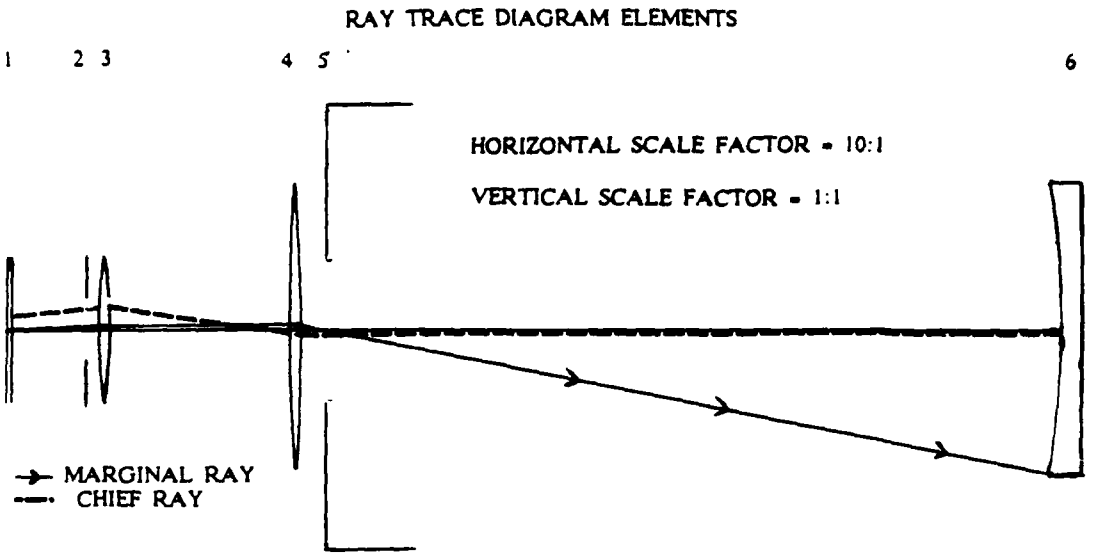

Ray Trace Diagram Parameters
(All lengths in millimeters; all angles in radians)

Element (Element #)	Physical dimension	Distance to next element	Focal length (power)	Marginal ray y-height w'-angle	Chief ray $\bar{y}$-height $\bar{w}'$-angle
Capillary (1)	H=4	115	NA	0 5.52E-3	2.00 1.30E-2
Slit aperture (2)	H=8	11	NA	6.35E-1 5.52E-3	3.49 1.30E-2
Collimating lens (3)	D=20.5	265	126.0 (7.94E-3)	6.96E-1 0	3.63 -1.59E-2
Focusing lens (4)	D=38.0	34.8	34.8 (2.87E-2)	6.96E-1 -2.00E-2	-5.72E-1 5.52E-4
Entrance slit (5)	H=19	1000	NA	0 -2.00E-2	-5.52E-1 5.52E-4
[Aperture Stop] Grating (6)	H=40	NA	1000 (1E-3)	-20.0 —	0 —

"Height" of fluorescing capillary = $2\bar{y}_1$ = 4.0 mm

Input optics to spectrometer: $F/\# = -\frac{1}{2w_1'} = \frac{1}{2(2.0E\text{-}2)} = 25$

Spectrometer: $F/\# = \frac{f_6}{D_6} = \frac{1000}{40} = 25$

Figure A2. Ray trace diagram (side view) of the spectrometer input optics.

APPENDIX B

GRATING GHOSTS AND SCATTERING

During our initial experiments with the spectrometer, we used pulse counting and current measurement by a linear picoammeter to detect PM signals. When spectra were recorded on a linear scale, signals that were more than two orders of magnitude lower than the intensity of the brightest spectral line were essentially "buried" in the noise. We therefore used a logarithmic picoammeter, which had equal resolution within each order of magnitude, to detect PM signals. This showed the spectra in more detail than had been previously observed with this spectrometer. This greater detail appeared as periodic false spectral lines surrounding any strong spectral line, broad bands on both sides of strong spectral lines, and exactly reproducible, spurious "spectra" from the 4416 Å HeCd laser in the wavelength region from 4300 to 6400 Å.

Figure B1 shows the periodic false spectral lines and broad bands (left band between 4360 and 4390 Å and right band between 4445 and 4470 Å) in a series of three measurements taken to study these features. The top figure was taken with the HeCd laser beam directed off-center toward the right side of the spectrometer's entrance slit, for the middle figure it was directed to the center of the entrance slit, and for the bottom figure it was directed toward the left side of the entrance slit. The periodic false spectral lines maintained their shape and relative wavelength separation, which ranged from 8.6 to 9.1 Å. However, the intensities of the broad bands changed relative to each other. This showed that the false spectral lines did not depend on the direction of the incident illumination, whereas the broad bands

did. Additional spectral scans taken with blocked portions of the grating, varying combinations of ground glass diffusers and neutral density filters, and different light sources supported these conclusions.

The periodic false spectral lines turned out to be grating, or Rowland, ghosts which arise from any type of periodic ruling error in the diffraction grating. Periodic errors are regions in the grating where the grooves are not perfectly straight, evenly spaced, parallel, or exactly identical in shape. These errors are caused by periodic ruling machine instabilities that occur while the grating is being ruled. Such instabilities can cause displacements of the groove cutting tool from the standard groove spacing and variations in groove depth and shape. The apparent wavelengths of the grating ghosts are given by $\lambda' = \lambda (1 \pm m'/mn)$, where λ is the spectral line's wavelength, m is the order, m' is the order of the ghost, and n is the number of grooves ruled in one turn of the screw.

Grating ghosts and the broad reflection bands are shown in Figure B2 for the HeNe laser (6328 Å) and the Hg blue line (4358 Å). The wavelength dependence of the grating ghosts is evident in the separation of the Hg blue line's ghosts (~8 to 10 Å), which is less than the corresponding separation of the HeNe line's ghosts (~12.5 Å). The broad band on the left side of the spectral line for the HeNe laser is more intense than the band on the right side, as it was for the HeCd laser. In fact, the broad band on the right side of the Hg blue line is barely visible.

The omnipresent HeCd laser "spectra" are shown between 4500 and 6300 Å in Figure B3. At 4700 Å, the intensity level decreases to approximately three orders of magnitude above the dark current noise level and remains relatively constant thereafter. At first glance the signal looks like noise. Three regions, indicated by boxes in Figure B3, are expanded in Figure B4 to show the HeCd signals are not noise, but signals that strongly resemble spectral lines. Region A

contains grating ghosts, and highlights the relative intensities of the ghosts and the "spectra". Regions B and C are two regions that were closely examined with optical bandpass filters. When filters that transmitted light only in these regions were used, the spectra disappeared. However, when a 4416 Å narrow bandpass filter was used, the spectra remained and were reduced in intensity by the filter's transmission efficiency.

Just as any surface scatters light into all directions, so too does the grating scatter the laser beam into all angles inside the spectrometer and not only in the angle of diffraction. Whenever the laser beam was scattered from the capillaries into the spectrometer, this background noise level was present with its exactly reproducible spectra.

The presence of the grating ghosts, broad bands, and spurious scattering were a surprising discovery and reason for concern until their causes were determined. (The scattered "spectra" were initially attributed to excited He and Cd atoms inside the laser medium.) These effects, while always present to some degree, can be disregarded or taken into account when the light from any source is spectrally analyzed and identified.

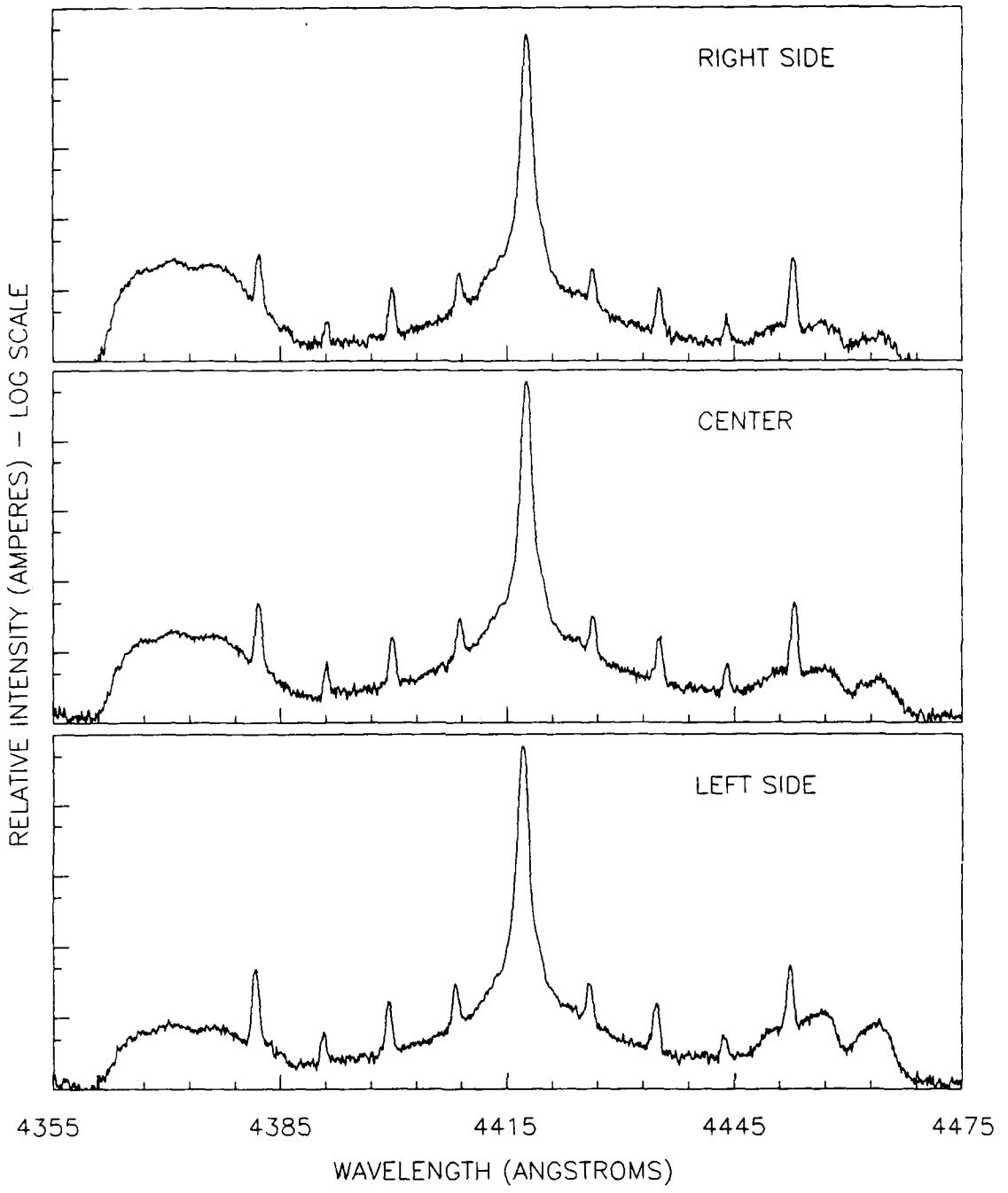

Figure B1. Grating ghosts and broad bands from the HeCd laser.

(Laser beam directed at right side, center, and left side of the spectrometer entrance slit to note directional effects.)

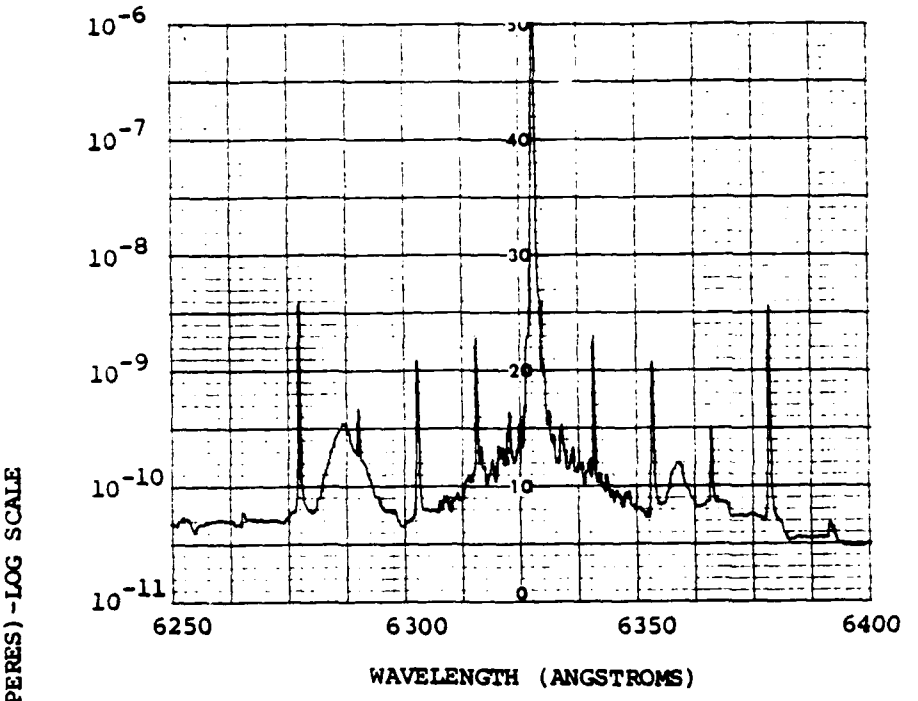

(A) HeNe laser (6328 Angstroms)

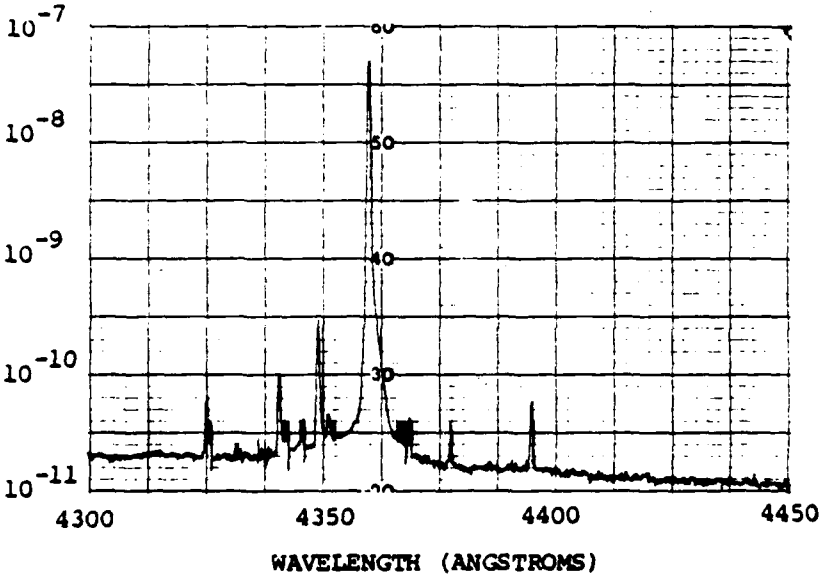

(B) Hg blue line (4358 Angstroms)

Figure B2. Grating ghosts and broad bands from HeNe laser and Hg sources.

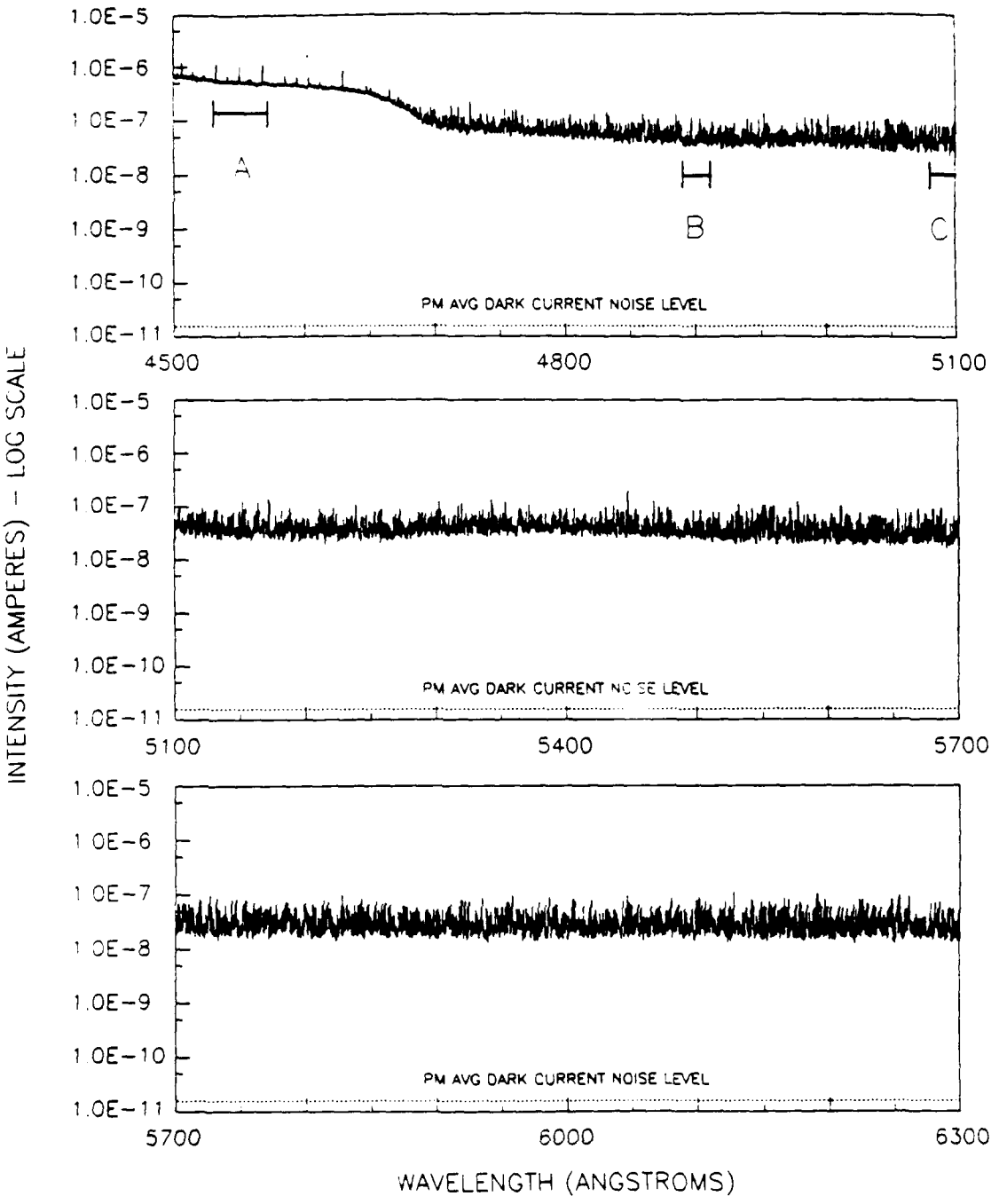

Figure B3. 4416 Angstrom "spectra" observed from the HeCd laser between 4500 and 6300 Angstroms. (|——| regions are expanded in Figure B4.)

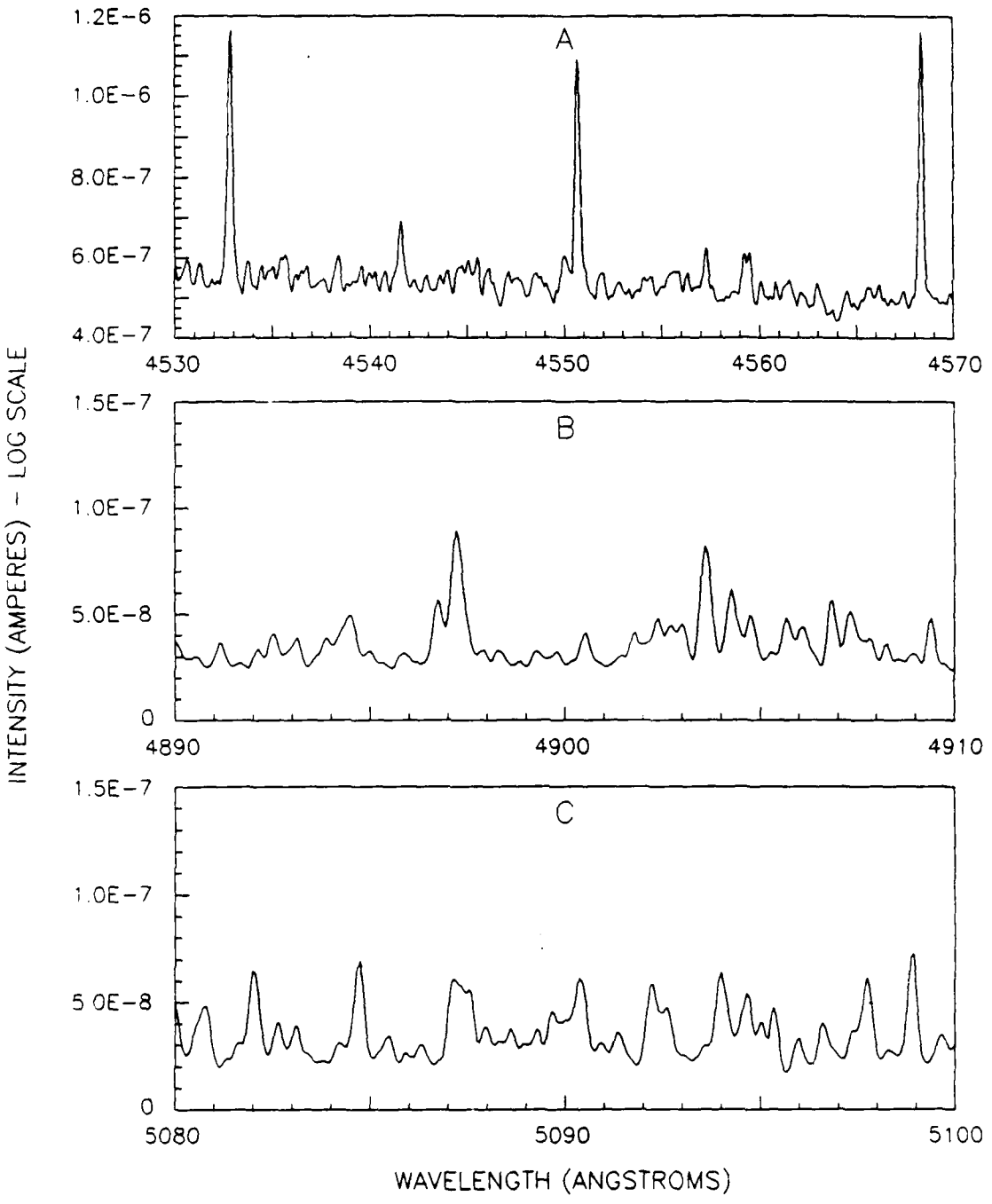

Figure B4. Expanded regions of the HeCd 4416 Angstrom "spectra" from Figure B3.

REFERENCES

1. J. S. Green, and J. W. Jorgenson, "Variable-Wavelength On-Column Fluorescence Detector for Open-Tubular Zone Electrophoresis," Journal of Chromatography, 352, 337 (1986).

2. R. A. Wallingford and A. G. Ewing, "Capillary Zone Electrophoresis with Electrochemical Detection in 12.7 μm Diameter Columns," Analytical Chemistry, 60, 1972 (1988).

3. B. W. Bell, "The Entire Scattering Matrix for a Single Fiber," M.S. Thesis, University of Arizona, 1981.

4. H. C. Van De Hulst, Light Scattering by Small Particles (John Wiley & Sons, Inc., N.Y., 1957).

5. R. E. Benner, P. W. Barber, J. F. Owen, and R. K. Chang, "Observation of Structure Resonances in the Fluorescence Spectra from Microspheres," Physical Review Letters, 44, 475 (1980).

6. S. Arnold and L. M. Folan, "Fluorescence Spectrometer for a Single Electrodynamically Levitated Microparticle," Review of Scientific Instruments, 57, 2250 (1986).

7. H.-B. Lin, A. L. Huston, B. L. Justus, and A. J. Campillo, "Some Characteristics of a Droplet Whispering-Gallery-Mode Laser," Optics Letters, 11, 614 (1986).

8. A. Biswas, H. Latifi, R. L. Armstrong, and R. G. Pinnick, "Time-Resolved Spectroscopy of Laser Emission from Dye-Doped Droplets," Optics Letters, 14, 214 (1989).

9. J. P. Kratohvil, M.-P. Lee, and M. Kerker, "Angular Distribution of Fluorescence from Small Particles," Applied Optics, 17, 1978 (1978).

10. H. Chew, P. J. McNulty and M. Kerker, "Model for Raman and Fluorescent Scattering by Molecules Embedded in Small Particles," Physical Review A, A13, 396 (1976).

11. H. Chew, M. Kerker, and P. J. McNulty, "Raman and Fluorescent Scattering by Molecules Embedded in Concentric Spheres," Journal of the Optical Society of America, 66, 440 (1976).

12. H. Chew, M. Sculley, M. Kerker, P. J. McNulty, and D. D. Cooke, "Raman and Fluorescent Scattering by Molecules Embedded in Small Particles: Results for Coherent Optical Processes," Journal of the Optical Society America, 68, 1686 (1978).

13. M. Kerker, P. J. McNulty, M. Sculley, H. Chew, and D. D. Cooke, "Raman and Fluorescent Scattering by Molecules Embedded in Small Particles: Numerical Results for Incoherent Optical Processes," Journal of the Optical Society of America, 68, 1676 (1978).

14. H. Chew, D. D. Cooke, and M. Kerker, "Raman and Fluorescent Scattering by Molecules Embedded in Dielectric Cylinders," Applied Optics, 19, 44 (1980).

15. J. F. Owen, P. W. Barber, P. B. Dorain, and R. K. Chang, "Enhancement of Fluorescence Induced by Microstructure Resonances of a Dielectric Fiber," Physical Review Letters, 47, 1075 (1981).

16. D. Abromson, "Fluorescence Enhancement and Angular Scattering by Selected Particles," Ph.D. Dissertation, University of Arizona, TBP, 1989.

17. E. Gassmann, J. E. Kuo, and R. N. Zare, "Electrokinetic Separation of Chiral Compounds," Science, 230, 813 (1985).

18. W. S. Bickel, "Optical system for light scattering experiments," Applied Optics, 18, 1707, 1979.

19. Vacuum Ultraviolet Scanning Spectrometer Instruction Manual, Jarrell-Ash Company, Waltham, Mass, pp. 30-39.

20. S. P. Davis, Diffraction Grating Spectrographs (Holt, Rinehart and Winston, N. Y., 1970), pp. 50-53.

21. Photomultipliers Manual, EMI Industrial Electronics LTD, Middlesex, England (1979), p.18.

22. G. A. Reynolds, and K. H. Drexhage, "New Coumarin Dyes with Rigidized Structure for Flashlamp-Pumped Dye Lasers," Optics Communications, 13, 222 (1975).

23. A. N. Fletcher and D. E. Bliss, "Laser Dye Stability. Part 5: Effect of Chemical Substituents of Bicyclic Dyes Upon Photodegradation Parameters," Applied Physics, 16, 289 (1978).

24. S. A. Tuccio, K. H. Drexhage, and G. A. Reynolds, "CW Laser Emission from Coumarin Dyes in the Blue and Green," Optics Communications, 7, 248 (1973).